University of Alberta

The Effect of Solution Composition on Erosion-Corrosion Process and Correlation between Repassivation Kinetics and Corrosion Rate in Flowing Slurry

by

Ke Wang ©

A thesis submitted to the Faculty of Graduate Studies and Research
in partial fulfillment of the requirements for the degree of

Master of Science
in
Materials Engineering

Department of Chemical and Materials Engineering

Edmonton, Alberta
Fall 2008

Library and Archives Canada

Published Heritage Branch

395 Wellington Street
Ottawa ON K1A 0N4
Canada

Bibliothèque et Archives Canada

Direction du Patrimoine de l'édition

395, rue Wellington
Ottawa ON K1A 0N4
Canada

Your file Votre référence
ISBN: 978-0-494-47437-2
Our file Notre référence
ISBN: 978-0-494-47437-2

NOTICE:
The author has granted a non-exclusive license allowing Library and Archives Canada to reproduce, publish, archive, preserve, conserve, communicate to the public by telecommunication or on the Internet, loan, distribute and sell theses worldwide, for commercial or non-commercial purposes, in microform, paper, electronic and/or any other formats.

The author retains copyright ownership and moral rights in this thesis. Neither the thesis nor substantial extracts from it may be printed or otherwise reproduced without the author's permission.

AVIS:
L'auteur a accordé une licence non exclusive permettant à la Bibliothèque et Archives Canada de reproduire, publier, archiver, sauvegarder, conserver, transmettre au public par télécommunication ou par l'Internet, prêter, distribuer et vendre des thèses partout dans le monde, à des fins commerciales ou autres, sur support microforme, papier, électronique et/ou autres formats.

L'auteur conserve la propriété du droit d'auteur et des droits moraux qui protège cette thèse. Ni la thèse ni des extraits substantiels de celle-ci ne doivent être imprimés ou autrement reproduits sans son autorisation.

In compliance with the Canadian Privacy Act some supporting forms may have been removed from this thesis.

While these forms may be included in the document page count, their removal does not represent any loss of content from the thesis.

Conformément à la loi canadienne sur la protection de la vie privée, quelques formulaires secondaires ont été enlevés de cette thèse.

Bien que ces formulaires aient inclus dans la pagination, il n'y aura aucun contenu manquant.

Canada

ABSTRACT

In the erosion-corrosion process, due to the interaction between mechanical erosion and electrochemical corrosion, a significant synergistic effect causes additional damage to target materials.

In the present work, the influence of chemical composition on erosion resistance and surface degradation of materials were investigated. The experimental data of the erosion-corrosion of carbon steel and *in-situ* nanoindentation indicate that erosion resistance and surface mechanical properties are largely dependent on the chemical composition of the materials.

Meanwhile, a theoretical model was developed to correlate and to quantitatively evaluate the average current density of carbon steel in flowing slurry. The impingement of solid particles in flowing slurry causes the breakdown of passive film. The enhanced anodic dissolution is dominated by the breakdown of passive film. The parameters of measured repassivation kinetics enable the prediction of the average anodic current density on the electrode surface in flowing slurry.

ACKNOWLEDGEMENT

I would like to thank all of the people who helped me with my M.Sc study.

Firstly, I would like to express my sincere appreciation of my supervisor, Professor Jingli Luo. Her guidance and encouragement really helped me throughout my two years' M.Sc study. She taught me how to think like a researcher. More importantly, she is an outstanding example for me. Her attitude and spirit in the career are treasures for me and they will help me in all aspects of my life.

Secondly, I am incredibly grateful to Dr. Baotong Lu. He trained me to act and think as a qualified master student. During my research, he always gave me great help to overcome my problems. Also, his wisdom and passion deeply impressed me. I always learned more than I expected, not all of it academic.

I also acknowledge NSERC (Natural Science and Engineering Research Council of Canada) for financially supporting this research.

Finally, I give special thanks to my parents and all of my friends. They always provided selfless help when I was in trouble. They gave me support and encouragement. Without them, I can not have had these two happy years.

TABLE OF CONTENTS

Chapter 1 Introduction 1

References 2

Chapter 2 Literature review 4

2.1 Analysis of weight loss 5
2.2 Individual processes of erosion-corrosion 7
2.2.1 Pure corrosion 7
2.2.1.1 Two different corrosion systems 8
2.2.1.2 Corrosion in flowing condition 9
2.2.2 Pure erosion 10
2.2.3 Synergistic effect 13
2.2.3.1 Effect of erosion on corrosion 15
2.2.3.2 Effect of corrosion on erosion 20
2.3 Factors that influence the erosion-corrosion process 24
2.3.1 Material properties 24
2.3.1.1 Microstructure 24
2.3.1.2 Compositions 26
2.3.1.3 Mechanical properties 26
2.3.2 Hydrodynamic properties 28
2.3.2.1 Flowing velocity 28
2.3.2.2 Particle concentration 29
2.3.2.3 Particle property 31
2.3.2.4 Impinging angles 31
2.3.3 Electrochemical parameters 32
2.3.3.1 pH of slurry 32
2.3.3.1 Corrosion current density 33
2.4 Topic selection 34
References 35

Chapter 3 Experimental Apparatus and Procedures 47

3.1 Materials 47
3.2 Experimental Setup and Procedures 50
3.2.1 Rotating cylinder electrode system 50
3.2.1.1 System description 50
3.2.1.2 Experimental procedure 52
3.2.1.3 Analysis of erosion-corrosion weight loss 53
3.2.2 Electrode scratch system 54
3.2.2.1 System description 54
3.2.2.2 Experimental procedure 55

3.2.3 Nanoindentation system 55
3.2.3.1 System description 55
3.2.3.2 Experimental procedure 57
3.2.3.3 The mechanism of nanoindentation 61
References 64

Chapter 4 The Effect of Solution Composition on Erosion-Corrosion and Surface Mechanical Properties of Fe Based Alloys and Iron 67

4.1 Introduction 67
4.2 Experimental details 67
4.3 Results 71
4.3.1 Erosion-Corrosion Material Loss Test 71
4.3.2 *In-situ* nanoindentation tests 76
4.4 Discussions 84
4.4.1 Relationship between erosion-corrosion and surface mechanical properties 84
4.4.2 Effect of solution compositions on erosion resistance and surface mechanical properties 87
4.5 Conclusions 88
References 88

Chapter 5 Correlation between Repassivation Kinetics and Corrosion Rate over a Passive Surface in Flowing Slurry 92

5.1 Introduction 92
5.2 Experimental details 93
5.3 Results 94
5.3.1 Corrosion current density in rotating slurry 94
5.3.2 Current decay in scratch test 98
5.3.3 Correlation between corrosion current density and repassivation kinetics 100
5.3.4 Calculation details and predicted results 105
5.4 Discussions 113
5.4.1 Measurements of repassivation kinetics 113
5.4.2 Galvanic effect 114
5.4.3 Mechanical properties of target materials and solid particles 115
5.4.4 Effect of repeated impingements of solid particles 115
5.4.5 Corrosion-enhanced erosion 116
5.5 Conclusions 117
References 117

Chapter 6 Summary and Future Work 121

6.1 Contribution to knowledge 121
6.2 Contribution to literature 122
6.3 Contribution to Engineering 123
6.4 Suggestions for future work 124

LIST of TABLES

Table 3-1 Chemical composition of A1018 and A1045 steels (wt%) 47
Table 3-2 Chemical composition of commercial pure iron (wt%) 48
Table 3-3 Chemical composition and mechanical properties of sand 48
Table 4-1 Solution compositions 68
Table 4-2 Acidic solution compositions 69
Table 4-3 Weight loss under cathodic protection (-0.9V_{SCE}) 73
Table 4-4 Weight loss under anodic dissolution (1 mA/cm^2) 74
Table 4-5 pH values of Group A and Group C 74
Table 4-6 Actual cathodic and anodic current densities when i_{ap} was 1 mA/cm^2 83
Table 5-1 Experimental conditions 93
Table 5-2 Test solutions 93
Table 5-3 Parameters of repassivation kinetics for carbon steels (τ_0=0.01s) 100
Table 5-4 Sand particle properties 100

LIST OF FIGURES

Figure 2-1 Schematic illustration of interaction in erosion-corrosion process 4
Figure 3-1 Microstructures of (a) A1018, (b) A1045 and (c) pure iron 49
Figure 3-2 Silica sand by SEM 49
Figure 3-3 Steel specimen for RCE system 50
Figure 3-4 Schematic set-up of rotating system for erosion-corrosion tests 51
Figure 3-5 Schematic set-up of electrode scratch system 54
Figure 3-6 Schematic set-up of indent cell for in-situ nanoindentation 56
Figure 3-7 Schematic set-up of in-situ nanoindentation system 56
Figure 3-8 Hardness of quartz under different loads 58
Figure 3-9 Reduced modulus of quartz under different loads 58
Figure 3-10 Indent load curves 59
Figure 3-11 Scratch load curves 60
Figure 3-12 Lateral displacement of scratch tests 61
Figure 3-13 Typical load depth curve 62
Figure 4-1 Typical indent image obtained in air, P = 1200 μN 70
Figure 4-2 Load-depth curves of pure iron in air 70
Figure 4-3 Contact depth with increasing load 70
Figure 4-4 Surface hardness with increasing load 71
Figure 4-5 Erosion-corrosion rates with increasing of anodic current densities 72
Figure 4-6 Erosion rates with increasing of anodic current densities 72
Figure 4-7 Erosion rates with increasing of anion strength 75
Figure 4-8 Contact depth with increasing of applied loads under CP 77
Figure 4-9 Surface hardness with increasing of applied loads under CP 77
Figure 4-10 Contact depth with increasing applied loads under AD 77
Figure 4-11 Surface hardness with increasing applied loads under AD 78
Figure 4-12 Surface morphologies in different conditions: (a) in air; (b) under cathodic protection in 0.1M Na_2SO_4; and (c) under anodic dissolution 80
Figure 4-13 Polarization curves in different solutions 82
Figure 4-14 Extrapolation method to determine cathodic current density 82
Figure 4-15 Contact depth measured under actual anodic dissolution 83
Figure 4-16 Surface hardness measured under actual anodic dissolution 83
Figure 4-17 Schematic illustration of single sand impingement 85
Figure 4-18 Friction coefficients with increasing contact depth 85
Figure 5-1 Polarization curves of (a) A1018 and (b) A1045 in slurries with different solution concentrations 95
Figure 5-2 Erosion-corrosion current densities with the solution concentrations of (a) and (c) 0.1 M, and (b) and (d) 0.3 M 97
Figure 5-3 Power law of the current decay of A1018 and A1045 steels 99
Figure 5-4 Gamma function 105
Figure 5-5 Craters created by sand impingements 108
Figure 5-6 Correlation between current density of A1018 and erosion rates 111
Figure 5-7 Correlation between current density of A1045 and erosion rates 113

LIST OF SYMBOLS

Symbols	Meanings
A	Surface area of electrode
A_s	Contact area made by the indent tip
$A(h_c)$	Area function calculated from contact depth
$\dot{A}_e$	Normalized fresh surface generating rate caused by the particle impingement
$\overline{A}_{crater}$	Average crater caused by every single particle impingement
B	Arbitrary fitting parameter fitted by indent curve
c	Weight loss rate caused by corrosion
c_0	Weight loss rate caused by pure corrosion
c_e	Weight loss rate caused by erosion-enhanced corrosion
C	Solution concentration
C_0	2.598
C_1 through C_5	Parameters obtained by nanoindentation calibration
C_p	Weight of solid particles
Cs	Sand concentration
$\bar{d}_p$	Mean diameter of particle
E	Potential
E_r	Reduced modulus
e	Weight loss rate caused by erosion
e_0	Weight loss rate caused by pure erosion
e_c	Weight loss rate caused by corrosion -enhanced erosion
F	Faraday constant
f	Friction coefficient
$f(\theta)$	Function about the dependence of erosion rate on impact angle
h	Indent depth
h_c	Contact depth
h_f	Arbitrary fitting parameter fitted by indent curve
h_{max}	Maximum indent depth
H	Hardness (GPa)
Hv	Vickers hardness of bulk material
ΔHv	Change in hardness due to anodic dissolution
i	Current density
$\bar{i}$	Average current density
i_a	Anodic current density
i_{ap}	Applied current density
i_c	Cathodic current density
i_{peak}	Peak current density

i_s	Stable passive current density
i_{th}	Threshold current density that causes surface mechanical degradation
J_p	Weight of solid particles
k_H	Experimental constant related to hydrodynamic conditions
m	Arbitrary fitting parameter fitted by indent curve
m_1 and m_2	Constants dependent on the erosion-corrosion system
$\overline{m}_p$	Average mass of sand particle
M_{Fe}	Molar weight of Fe (56g/mol)
M_p	Weight of particles per unit volume of solution
n	Experimental constant related to erosion systems
n_H	Experimental constant related to hydrodynamic conditions
n_i	Impingement frequency over an electrode surface with unit area
P	Applied load
$P_{\max}$	Maximum load
S	Calculated stiffness of target material at peak load
t	Time
t_{RP}	Repassivation time
u	$u = \dot{A}_e t$
U	Flowing velocity
$\overline{V}_p$	Average volume of sand particle
w	Total weight loss rate
w_s	Weight loss rate caused by synergistic effect
$\overline{w}_{crater}$	Crater width
$\overline{w}_{crater,AP}$	Crater width under anodic dissolution
$\overline{w}_{crater,CP}$	Crater width under cathodic protection
y	$y = \overline{A}_{crater} / \overline{V}_{crater}$
z	Valence of Fe
Z	Constant that varies with systems
α and β	Fitted experimental constants by repassivation curve
ε	Geometric constant related to shape of the tip
θ	Impingement angle
λ	$\lambda = \tau \dot{A}_e$
λ_0	$\lambda_0 = \tau_0 \dot{A}_e$
μ	Experimental constant
ρ	Density of Fe
ρ_p	Density of sand particle
τ	Current decay constant
τ_0	0.01s

ω	**Angular velocity**
Λ	dA/A

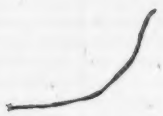

Chapter 1

Introduction

Erosion-corrosion is a complicated process that causes failures of coal-slurry pumps and pipelines in the petroleum and mining industries [1]. Erosion, in corrosion media, always accomplished with chemical attack results in the combination of two material loss processes: electrochemical dissolution in a corrosive environment and mechanical wear due to the impingement of solid particles. As a chemical reaction, corrosion leads to the change on the surface of materials, such as pitting and degradation of hardness on the surface. Meanwhile, erosion defined as a mechanical process, rubs off the material on the surface. These two effects interact almost simultaneously in the mixture of liquid and solid, resulting in synergism of erosion-corrosion. This indicates that material loss due to erosion-corrosion is not simply the summation of independent corrosion and erosion. The additional material loss occurs when these two processes take place simultaneously, i.e. material loss caused by corrosion-enhanced erosion and erosion-enhanced corrosion [2,3,4,5,6]. Many studies have been based on the investigation of the synergistic effect, and they have pointed out that the erosion rate of a material would be remarkably increased with the presence of a corrosion

current, even if the corrosion current was too small to be measured [7,8,9]. Therefore, it is important to investigate the mechanisms of erosion-corrosion and the interaction between them.

In order to provide effective solutions to lower the potential risk of erosion-corrosion and to extend the service life of tailing pipelines, it is important to understand the phenomenon. It is also important to reveal the mechanism of interaction between erosion and corrosion, and to investigate the factors that influence the erosion-corrosion process.

In this case, the objective of this research is to investigate the effect of the solution composition on the erosion-corrosion process and the surface mechanical degradation. In addition, a theoretical model was proposed to correlate the average current density with repassivation kinetics for passive systems.

References

[1] R. Babu, S. Bhaskar, K. Chockkalingam, G.T. Parthiban, N.S. Rengaswamy, "Erosion corrosion of HSLA steel in a coal slurry", Corrosion Prevention and Control, v43, n5 (1996), pp. 131-134.

[2] B.T. Lu, J.L. Luo, "Synergism of electrochemical and mechanical factors in erosion - corrosion", Journal of Physical Chemistry B, (2006), pp. 4217-4231.

[3] B, T. Lu, J. L. Luo, "Prediction of Synergistic Effect in Erosion Corrosion", submitted to Corrosion Science (2007).

[4] H.X. Guo, B.T. Lu, J.L. Luo, "Response of surface mechanical properties to electrochemical dissolution determined by in situ nanoindentation technique", Electrochemistry Communications, v8, pp. 1092-1098.

[5] H.X. Guo, B.T. Lu, J.L. Luo, "Interaction of mechanical and electrochemical factors in erosion-corrosion of carbon steel", Electrochimica Acta 51 (2005), p. 315-323.

[6] M.M. Stack, B.D. Jana, "Modelling particulate erosion-corrosion in aqueous slurries: Some views on the construction of erosion-corrosion maps for a range of pure metals", Wear, v256 (2004), pp. 986-1004.

[7] M. Matsumura, Y. Oka. Proceedings of the 7th International Conference on Erosion by Liquid and Solid Impact, Cavendish Laboratory, University of Cambridge, Cambridge, UK (1987).

[8] Z. Yue, P. Zhou, J. Shi, "Some factors influencing corrosion-erosion performance of materials", Wear of Materials, ASME, New York (1987), pp. 763-768.

[9] Y. Zheng, Z. Yao, X. Wei, W. Ke, "Synergistic effect between erosion and corrosion in acidic slurry medium", Wear 186-187 (1995), pp. 555-561.

Chapter 2

Literature Review

Erosion-corrosion causes severe damage in slurry transportation and other related industries every year [1]. Many groups from both academia and industry put their efforts toward investigating the mechanism of erosion-corrosion and how to prevent or reduce its effect.

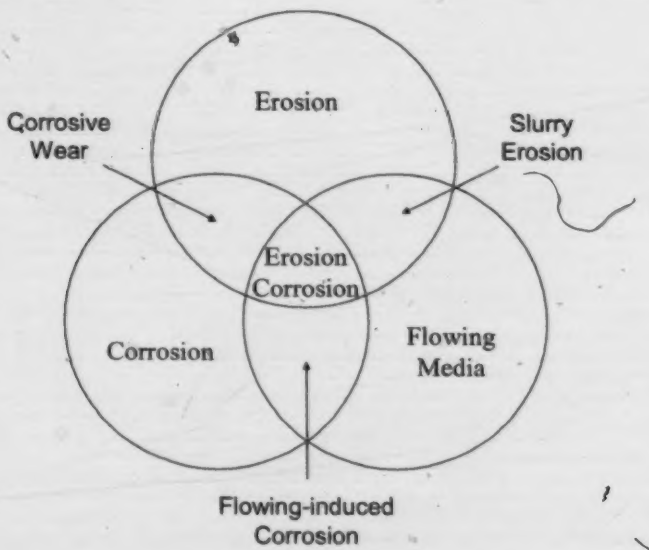

Figure 2-1 Schematic illustration of interaction in erosion-corrosion process

In erosion-corrosion, there are three single processes: the impingement of solid particles, electrochemical reactions, and the flowing of the media. These

processes interact with each other and make erosion-corrosion quite a complicated phenomenon. **Fig. 2-1** shows the interactions between erosion, corrosion, and flowing media. This indicates that erosion-corrosion processes exist only with the coexistence of erosion, corrosion, and a flowing media.

2.1 Analysis of weight loss

In order to investigate the erosion-corrosion process, weight loss is always used to evaluate erosion-corrosion resistance. The total weight loss rate, w, is divided into two major parts: mechanical erosion rate, e, and electrochemical corrosion rate, c [2,3,4,5,6]. Their relation is shown in **Eq. 2-1** [3,4,5,6]:

$$w = e + c \tag{2-1}$$

To further investigate the entire process, the mechanical erosion, e, is divided into the pure erosion rate, e_o, and the corrosion-enhanced erosion rate, e_c as in **Eq. 2-2**. The electrochemical process is similarly divided into the pure corrosion rate, c_o, and the erosion-enhanced corrosion rate, c_e as in **Eq. 2-3**.

$$e = e_0 + e_c \tag{2-2}$$

$$c = c_0 + c_e \tag{2-3}$$

The total weight loss rate is therefore:

$$w = e + c = e_0 + e_c + c_0 + c_e \tag{2-4}$$

Eq. 2-4 indicates that the weight loss caused by erosion-corrosion is not simply a summation of the pure corrosion and the pure erosion. There is an additional weight loss in the erosion-corrosion process. This additional weight loss is caused by the synergistic effect of erosion and corrosion, which is called the synergistic weight loss, w_s as in **Eq. 2-5** [7].

$$w_s = e_c + c_e \tag{2-5}$$

Due to the interaction between erosion and corrosion, the two processes are accelerated and the weight loss caused by this synergistic effect is always larger than zero. Some researchers even found that the synergistic effect could account for as much as 80% of the total weight loss [8,9]. When studying the process of erosion-corrosion, researchers should put their efforts into investigating the synergistic effect, in addition to erosion and corrosion.

2.2 Individual processes of erosion-corrosion

Erosion processes include cutting, plastic deformation, or contact fatigue caused by the cavitation of flowing fluid or the impact of solid particles [10]. Thus, it has the nature of a mechanical degradation process. The corrosion process is the dissolving of a material's atoms by an anodic current. The material's atoms dissolve into the solution in their ionic form. This process has the nature of an electrochemical process. Together, these two processes cause the additional synergistic effect and result in a complicated problem. Therefore, in order to investigate this problem, it is necessary to understand the individual processes involved in erosion-corrosion.

2.2.1 Pure corrosion

Bradford [11] defined corrosion as "the damage to metal caused by reaction with its environment". Corrosion always takes place on the metal's surface where it is in contact with its environment, such as soil, a solution, or even humid air. Thermodynamically, when in contact with an environment, most metals are unstable. They have a tendency to lose their electrons and convert to more stable forms, i.e. cations, oxides or other chemical compounds [12]. It is like the reverse of extractive metallurgy.

As mentioned above, in the corrosion process, there is charge transfer, hence it is an electrochemical process. When corrosion takes place, metal atoms interact

with the solution. In most cases, there are three basic steps to this process: a) the transportation of the reactant to the electrode surface; b) a surface electrochemical reaction; c) the transportation of the product away from the electrode surface. Each step is quite complicated. For example, when the metal atoms interact with the reactant, there is atom adsorption, the first electron discharge, formation of complex ions with other species, and then further discharging into the final product [13].

2.2.1.1 Two different corrosion systems

The corrosion system can be divided into two major parts, based on whether the surface of the material is covered by a protective film. One is the active or non-passivated system and the other is the passive system.

In an active system, the surface of the material is not covered by a protective film. This system always experiences uniform corrosion. When the metallic atoms react with the electrolyte, some products may form on the surface. Generally, these products are not compact and non-protective. This indicates that the metallic atoms can dissolve into the electrolyte without any significant barriers. Galvanic corrosion, intergranular corrosion, and crevice corrosion occur in the active system. In this system, the controlling step is the charge transfer at the metal's surface or the mass transfer resistance in the fluid environment, or both.

In the passive system, the material's surface is always covered by a protective oxide film. This protective film can be either an adsorption film or a

three-dimensional oxide film. The passive film can lower the corrosion rate by preventing contact between the material's surface and the electrolyte, or by limiting the mobility of atoms and ions. Hence, the structure and properties of the passive film would influence the material's corrosion behaviour. The passive system always has a lower corrosion rate than the active system. However, in this system, localized corrosion always occurs and causes severe damage, i.e. pitting corrosion. For example, in pitting corrosion, pitting occurs in the pitting zone but the rest of area is still covered by the protective film, and therefore not corroded. This is typical of systems with a small anode and a large cathode, hence significantly increases the anodic dissolving rate [13]. With time, the pitting becomes deeper and deeper, and finally penetrates the entire material.

2.2.1.2 Corrosion in flowing condition

In a corrosive environment, flow influences corrosion rates. A flowing environment enhances mass transfer, hence increasing the total corrosion rate. The presence of a flowing medium increases corrosion rates when material is experiencing uniform or general corrosion. At high enough velocities, flow can hinder the formation of adsorbed films, or the passivation process. The metallic material itself may suffer mechanical damage at high enough fluid velocities [14,15,16].

2.2.2 Pure erosion

Erosion is surface damage caused by recurring localized trauma, i.e. by suspended abrasive particles in a flowing media. Erosion can also occur in a flowing media without abrasive particles, i.e. cavitation.

During the past fifty years, many researches have been devoted to investigating the mechanisms of erosion, and a number of erosion models have been proposed. In 1995, Meng and Ludema [17] conducted a thorough review of various erosion models. All of the proposed dominant models involve several common characteristics: a) a single hard particle impinges on a planar surface; b) erosion includes micro-mechanical deformation or fracture processes; c) the applicability of models depends on whether the target material can be described as ductile or brittle, and on the impingement angle of the hard particle. Several dominant models are described here.

Finnie [18,19] investigated the erosion of ductile metals and proposed a micro-cutting model. There are several assumptions in this model: a) when approaching the eroding surface, the particle removes material like a cutting tool at the eroding surface at a certain impingement angle; b) surface materials deform plastically during the cutting process; c) the impinging particles are much harder than the target materials. Based on those assumptions he proposed that the volume of removed materials can be calculated from the impinging particles' size and inertia trajectory.

However, Finnie's model has its limitations. The model was first proposed for ductile materials, and is therefore only applicable to ductile materials. Secondly, experimental data showed that this model is only suitable for predicting the erosion rate at impingement angles under 45°, while it would underestimate the erosion rate at angles greater than 45°. Finnie ascribed this discrepancy to the effects that the roughened surface and caused changes to the local impingement angles and rotation of impingement particles.

By examination of the erosion surface, some researchers concluded that the cutting tool analogy is not the primary mechanism of the erosion of ductile metals [20,21]. Bitter [22] proposed a deformation model, created by combining the effects of cutting wear and deformation wear. He has improved Finnie's model. The erosion of materials is not only a cutting process, but it is also a process of deformation. These two processes exist simultaneously. Meanwhile, he proposed a new concept: the threshold velocity of erosion. In this concept, the impingement of particles can remove material only if the impinging velocity is greater than this threshold velocity. When the velocity is lower than the threshold velocity, only elastic deformation will occur. This deformation will recover when the particles leave the material's surface. When the velocity is greater than threshold velocity, both elastic and plastic deformation will happen, and plastic deformation would not recover, hence inducing damage to the surface.

This model gives a prediction similar to Finnie's model when the material is

ductile. For hard or brittle materials, Bitter's model successfully predicts the maximum erosion rate at an angle of up to 90°, while Finnie's predicted zero at 90°, which is not correct.

Sundarajan and Shewmon [23] proposed the localization model. It states that during normal impingements, the critical strain should be reached before the target material is removed. It assumes that the solid particle impacts the surface. A localized lip of material is formed along the rim of the crater. When the critical strain reached, the formation of the localized lips occurred. This model showed a better agreement to the experimental data [24], but will still overestimate the erosion rate for some steels.

From the observations received through experiments, Hutchings [25] found that the erosion debris of material at a normal incidence was typically like flat platelets. From analysis of the debris, he observed that the debris was produced by many cycles of plastic deformation instead of a single or small number of impacts. Based on the cyclical plastic deformation, he developed a fatigue model and this model was treated as a cyclical fatigue problem. He proposed that the impact of a target material by impinging particles would cause erosion only if a critical threshold strain was reached, similar to the assumption of Sundarajan and Shewmon model [23].

This model considers both the dynamic hardness of material and ductility in the process of erosion, but not their initial mechanical properties. Hutchings' model

successfully shows a relationship between the velocity of impinging particles and the erosion rate. The proposed velocity exponent was found to agree reasonably with experimental data. However, there are several flaws with his assumptions. Firstly, he did not consider the effect of strain hardening. Secondly, the model assumes that the dynamic hardness of the material is constant during the erosion process. From this point of view, every impact of particle has the same effect on the strain increment. This is not correct, since the work hardening effect by impacts of particles would increase the surface hardness of materials during erosion process. Thirdly, it is difficult to apply this theory for the prediction of the erosion rate since it is difficult to determine the critical strain to fatigue life. Furthermore, it only considers the plastic deformation during the erosion process. It does not consider other mechanisms such as how the removal takes place.

2.2.3 Synergistic effect

From **Eq 2-4**, it can be concluded that the erosion-corrosion rate is higher than the summation of pure erosion and pure corrosion individually. The additional material loss rate is caused by the interaction between erosion and corrosion. Many researches have been based on investigation of the synergistic effect of erosion-corrosion. Matsumura *et al.* [26] reported that in a NaOH slurry, the material loss of pure iron with presence of a corrosion current was 20% higher than it was without corrosion, even though the corrosion current was too small to be

measured. Li *et al.* [27] investigated the material loss of aluminium in an acid slurry containing 0.5M NaCl and found that the synergistic effect accounted for 40-50% of the total weight loss. Yue *et al.* [8] reported that as much as 86% of the total weight loss of chrome white iron in low-pH slurry could be attributed to the synergism of erosion-corrosion. Zheng *et al.* [9] discovered that the weight loss due to this synergy could be as high as 92.1% for X60 pipe steel, 94.6% for 321 stainless steel, and even 99.8% for 316L stainless steel. A significant synergistic effect has been found in the investigations shown above. This means that it is important to investigate the phenomenon and mechanism of synergistic effect of erosion and corrosion.

In order to investigate the interaction between erosion and corrosion, Lim and Ashby [28,29] developed a wear map. This map illustrates the main wear parameter that dominates the material damage. Furthermore, Stack and Pungwiwat [30] improved this erosion-corrosion map to indicate whether erosion or corrosion dominates the material loss. The relationship between erosion-corrosion rate and major parameters are established under different conditions, such as flow velocity, sand concentration, applied potential, etc. The map ends with the extreme conditions of pure erosion and pure corrosion. Between these two extreme conditions, two regimes of different synergistic effects are located: corrosion-enhanced erosion and erosion-enhanced corrosion. Each particular regime is calculated by ratios of erosion rate to corrosion rate:

erosion dominated	$c/e < 0.1$
erosion-corrosion	$0.1 \leq c/e < 1$
corrosion-erosion	$1 \leq c/e < 10$
corrosion dominated	$c/e \geq 0.1$

The method of creating erosion-corrosion in aqueous slurry has been discussed in several papers [2,31,32,33,34,35,36,37]. This method could be used either to determine the relationship among w, e_o, c_o, e_c and c_e [35,36] or be applied to establish erosion-corrosion models [2,34,37].

Even though the erosion-corrosion map has been established, it can only quantitatively describe the erosion rate, the corrosion rate, and the ratio between them. It can not explain how erosion and corrosion interact with each other, or the mechanism of the synergistic effect. Many efforts have been made on investigation of the mechanism of erosion-corrosion, but due to its complexity, it is still not well understood. Mainly, researchers divided the synergistic effect into the effect of erosion on corrosion and corrosion on erosion, or the erosion-enhanced corrosion effect and the corrosion-enhanced erosion effect respectively.

2.2.3.1 Effect of erosion on corrosion

As mentioned above, effects of the erosion process include the flowing of

corrosive media and impingement of particles. In a passive system, these effects would result in roughing the surface, accelerating the mass transfer, breaking down the passive film, and promoting localized corrosion. In an active system, they would cause the above results except the break down of the passive film, because there is no passive film in an active system.

Roughening surface

The impingement of particles roughens the electrode surface. Normally, the rougher surface would result in a higher corrosion rate [38,39]. When the electrode surface is impinged by the particles for a single crater, a valley and a peak would form. Li *et al.* [38,39] used copper as the working electrode and investigated the electron behaviour of copper. They point out that it is easier for an electron to escape from the surface at the peak than that at the valley. This indicates that the peak is more easily corroded than the valley. For the overall roughened surface, there is a higher electron fluctuation and it has more freedom to react with its environment, hence it is more electrochemically active. Additionally, as the peak has a higher tendency to lose electrons, it is more active. In contrast, the valley is nobler. This implies that a galvanic couple would form, i.e. the peak acts as the anode and the valley acts as the cathode. Therefore, the local cell would be promoted, and would accelerate the corrosion process.

Burstein *et al.* [40] investigated the relationship of surface roughness and

pitting potential for stainless steel 304L and found out that the surface condition was a critical parameter in determining the pitting potential. It was proposed that surface roughness caused by erosion would also lower the pitting potential. He also found that during the erosion process, the pitting potential dropped more than it did after the erosion process. This indicates that beside surface roughness, there are some other parameters that influence the pitting potential.

Breakdown of passive film

As mentioned above, for a passive system, the surface of the material is covered by a compact oxide film, which prevents contact between the material surface and its environment. In the erosion process, the surface of the passive film might be damaged by impingement of particles or the cavitation effect. In this case, the fresh material surface is exposed to the corrosive environment, leading to additional corrosion damage. Lu *et al.* [6,41] investigated the single impact of sand particles. They reported that when the passive film is broken down, there is a high current response. After the impingement, the fresh material surface is repassivated quickly and is covered by a protective passive film once again. Li *et al.* [42] and Guo *et al.* [43] used a scratch test to simulate the effect of sand impingement, and received similar results to those obtained by single particle impingement. Guo *et al.* [43] also investigated the passive system of AISI 1045 carbon steel in different concentrations of borate buffer solutions, and found that in the sand slurry, the total

current increase is remarkably higher than it was without sand. Some researchers [44,45,46,47] reported that if the concentration or velocity of the slurry was high enough, it could alter the corrosion behaviour, i.e. eliminating passive zone.

The breakdown of the passive film could also enhance pitting corrosion. When a particle impinges on a material's passive surface, it rubs off the passive surface, and generates small pits. Burstein *et al.* [48,49] investigated this effect on stainless steel and found that the metastable pits can ensue immediately below the pitting potential after a short time. It increases the frequency of metastable pits, compared to the erosion-free condition. Also, these small pits might shorten the starting period of pitting corrosion, and the impingement of particles forms an occlusion for propagation of the small pits that were created into larger ones [50].

However, some researchers reported contradictory results. Renard [51] investigated the pitting corrosion behaviour of AISI 304L stainless steel and found that the pitting corrosion was slightly inhibited by the erosion of sand particles. He explained that the reason might be that the impingement of sand particles breaks down the occlusion environment and stops the propagation of pitting behaviour, hence inhibiting the pitting corrosion.

Accelerating mass transfer

For a corrosion process, there are always two reactions: a cathodic reaction and an anodic reaction. When the electrolyte is flowing, it increases the mass

transfer of oxygen, increasing the cathodic reaction rate and promoting the whole corrosion process [52]. Also, the flowing of solid particles in a solution results in a disturbance of the fluid. Therefore, it may increase the transportation processes of both reactants and corrosion products [9,16].

Strain hardening effect

When the sand hits the material surface with a high enough kinetic energy, it causes both elastic and plastic deformation on the surface. This process induces a deformation effect, such as a dislocation network, deformation bands, or emerging slip steps at the surface [53]. Li *et al.* [54] investigated the relationship between the strain rate effect and the electron work function, and pointed out that a higher strain rate would make it easier for electrons to escape from the material's surface, giving it an increased tendency toward corrosion. Li *et al.* [55] also investigated the change of current density of stainless steel's effect on strain rate in 10% H_2SO_4, and found that the current increased with the strain rate. Mayuzumi *et al.* [56] found that cold work would affect the corrosion behaviour of 304 stainless steel.

However, there might be some contradictory results regarding the strain effect and cold working. Lu *et al.* [57] investigated the strain effect of 304 stainless steel and found that in the pseudo-static deformation process, neither elastic nor plastic deformation would remarkably change the corrosion rate of the working electrode when it was experiencing an anodic dissolution process. Mayuzumi *et al.* [56] also

found that the effect of strain on corrosion is largely dependent on systems. In Li's investigation [55], it is difficult to tell whether it is the disruption of the passive film of stainless steel caused by tensile stress or the strain rate itself that increased the current.

2.2.3.2 Effect of corrosion on erosion

Corrosion is a chemical process, specifically the dissolving of a material's surface layer. When sands impinge on the surface, the erosion process will carry out more easily than erosion without any corrosion current, and this results in lowering the erosion resistance on the material's surface layer [2,3,4,5,6]. Processes such as roughing the surface, preferential dissolution of the matrix phase, removal of work hardened surface, vacancy generation, and chemo-mechanical effect will be discussed in this section.

Roughening surface

As the materials' micro structure is not perfectly uniform, the dissolution process on the surface of these materials is not uniform. Some areas are more sensitive to corrosion, while other areas are not. As a result, the more active areas act as the anode and the nobler areas act as the cathode. Thus, the anode experiences metallic dissolution, while the cathode does not. In this case, roughening occurs. Postlethwaite [58] investigated the erosion-corrosion behaviour of pipelines in an

aqueous slurry with and without an inhibitor. The inhibitor could reduce the corrosion process. He found that the erosion-corrosion rate and surface roughness could be reduced by adding an inhibitor. Some researchers [10,20] explained that, as the erosion process is sensitive to the impinging angles, the corrosion would change the impinging angles by roughening the surface.

Preferential dissolution of matrix phase

For some materials, the mechanical properties are reinforced by a dispersed second phase metal matrix composite (MMC) [59]. For example, the reinforced phase may increase the surface hardness of MMC, and could make the material more resistant to adhesion friction and abrasion friction, similar to the carbide drill which uses a cobalt matrix reinforced by hard tungsten carbide [59]. For these materials, the mechanical properties are largely dependent on the reinforced phase. When these materials are experiencing erosion-corrosion, the preferential dissolution always occurs on the junction sites of the matrix and the renforcement, because it is more galvanically active, hence more sensitive to corrosion [60,61]. This preferential dissolution weakens the binding of the composites and the metallic matrix. Thus, the reinforced composites may be more easily removed by erosive particles. This effect would cause the degradation of mechanical properties of the material's surface, hence lowering the erosion resistance of materials [62].

Removal of work hardened surface

Some materials have a high work-hardening ability. When the erosion process occurs, erosive particles keep hitting the material's surface, like inducing cold work on the material surface. This cold work induces a work hardening effect on the surface, and protects the material from further material loss caused by erosion or lower the erosion process [59]. Matsumura *et al.* [26] investigated the erosion-corrosion process in a passive system and pointed out that the impingement of particles rubs off the protective passive film and promotes the corrosion process. This corrosion current dissolves the work-hardened layer on the material surface, hence lowering the erosion resistance.

Generation of vacancies on surface layer

The preferential dissolution theory can explain the mechanical degradation of matrix composite materials, but it can not be applied to explain the mechanical degradation of single phase materials. Some researchers also investigated the erosion-corrosion process for single phase materials. Guo *et al.* [4] investigated the mechanical degradation of pure iron in the condition of anodic dissolution in solution by *in-situ* nanoindentation, and found that the surface hardness dropped considerably more in the presence of a corrosion current compared to that under cathodic protection condition. Matsumura *et al.* [26] reported that in a NaOH slurry, the material loss of pure iron with the presence of a corrosion current was 20% more than that without corrosion, even though the corrosion current was too small

to be measured. Jones *et al.* [63,64,65] proposed a vacancy generation theory to explain this effect for single phase materials. When a material is experiencing anodic dissolution, the supersaturation of vacancies is formed in the subsurface by anodic dissolution. The large amount of vacancies consequently causes weakening of inter-atomic bonds of the metal surface. The inter-atomic bonds induce a chemical potential gradient between the surface layer and the bulk material, which causes an anodic dissolution-induced dislocation flux in the surface layer. The vacancies generated during electrochemical dissolution are attracted to dislocations and increase their mobility. This enhanced mobility of dislocations decreased the resistance of the surface layer against plastic deformation [63,64,65]. Others [66,67,68,69] have also pointed out that the weakening of inter-atomic bonds at the metal surface will cause deterioration of the mechanical properties of the material, such as tensile strength, modulus, and fatigue life, hence lowering the erosion resistance. The erosion resistance is reduced in this fashion.

The vacancies caused by corrosion also induce a chemo-mechanical effect. The chemo-mechanical effect occurs when a load is applied on to a material's surface when a chemical reaction is occurring. The mechanical properties would be affected by this. Rehbinder [70] investigated the chemo-mechanical effect of lead, tin, and copper, and reported that when in contact with small amounts of surface active substances, the samples exhibited accelerated plastic flow. Gutman [71] pointed out that at the surface of a metal, the chemical or electrochemical metallic

dissolution would result in lowering its free energy and increasing the mobility of additional dislocation generated in this process, hence decreasing the resistance to plastic deformation. Jones *et al.* [63,64,65] and Gu *et al.* [72] proposed that the anodic dissolution would induce a supersaturation of vacancies at the surface of the metal. These vacancies would then diffuse to grain boundaries and isolate dislocations, leading to accelerated diffusion creep and dislocation climb.

2.3 Factors that influence the erosion-corrosion process

As mentioned above, erosion-corrosion is defined as the interaction of the impingement of solid particles, flowing media, and corrosion. It is an cross field study in material, hydrodynamic, and electrochemical properties. Therefore, the factors that influence each process affect the erosion-corrosion process.

2.3.1 Material properties

2.3.1.1 Microstructure

Erosion-corrosion resistance is largely dependent on phase composition and grain size [73,74,75,76]. Wang *et al.* [73] investigated the erosion-corrosion behaviour of carbon steel and found that a low-banitic microstructure could increase the erosion resistance of carbon steel. Peterson *et al.* [74] investigated different microstructures' effect on carbon steels at most angles of impingement and found

that their erosion resistances, ranked in order of increasing erosion rate, is as follows: spheroidite, pearlite, tempered martensite, and martensite. Lindsley *et al.* [75] reported that for spheroidized Fe-C alloys, erosion resistance increased when the mean free path between both the carbides and the grain boundaries decreased. Bregliozzi [76] reported that erosion resistance is also dependent on grain size, and the erosion resistance increases as the grain size decreases.

Metal matrix composites could also reinforce a material's mechanical properties, and increase the erosion resistance of materials [52,77,78,79,80]. Erosion-corrosion resistance is largely dependant on the corrosion resistance of materials, since corrosion tends to occur on the matrix. When a matrix has a relatively low resistance to corrosion, the hard particles embedded in that matrix are more easily removed by erosion. The erosion-corrosion resistance of MMCs is also dependent on the size and volume fraction of the hard particle phase [52,77,78,79]. Chaklader [81] pointed out that the wear resistance of a composite increases as its particle size decreases. However, regarding volume fraction, there are contradictory conclusions. Lindsley *et al.* [75] and Chuang *et al.* [77] reported that the erosion resistance increases with hard particle content, while Trazaskoma *et al.* [78] and Levin *et al.* [79] found the opposite to be true. Pugsley *el al.* [82] studied the eroded surface by microscopic examination and explained that this difference was due to their different material removal mechanisms.

2.3.1.2 Compositions

Generally speaking, increasing the carbon content increases the erosion resistance of carbon steel, but decreases its corrosion resistance [10,83,84]. For alloy steels, the addition of alloy elements, such as Cr, Mo, Mn, and Ni, improves the alloy's erosion-corrosion resistance [85,86,87,88]. Samy [89] reported that higher Cr alloy steel has a better erosion-corrosion resistance, due to Cr increasing both corrosion resistance and mechanical properties. Also, Lu *et al.* [90] investigated the effect of chemical composition on corrosive wear performance of cast chromium white irons, and built a map to identify the effect of alloy composition on corrosive wear. He indicated that the corrosion resistance of cast chromium white irons was dependent on the Cr content in its matrix [90].

2.3.1.3 Mechanical properties

Mechanical properties such as hardness, toughness, strength, and strain hardening ability influence the erosion-corrosion rate by changing its erosion behaviour. Many of the erosion models mentioned above are primarily established by the destruction of those mechanical properties. Hardness is a considerably important parameter and attracts lots of research interest in erosion-corrosion field.

Generally speaking, an increase of hardness results in a decrease of erosion. Many researchers created erosion models, and they all indicated that the erosion rate is inversely proportional to the hardness of the material [19,25,91,92]. The

equation is as follows:

$$e_0 = \kappa_H Hv^{-n_H} \tag{2-6}$$

where k_H and n_H are experimental constants and are related to hydrodynamic conditions. Hv is the hardness of the bulk materials. Oka *et al.* [92] pointed out that it is not the initial hardness of the materials that influences the erosion process: it is the hardness during the erosion process that influences the erosion, i.e. work-hardening effect. Hutchings [10] investigated the erosion behaviour of a wide range of materials and summarized that the erosion rate depends heavily on the hardness difference between the target material and that of the impinging particles. Finnie [19] also investigated a wide range of materials and found that the erosion rate is inversely proportional to the hardness, in which the power constant is 1. However, some researchers also pointed out that the erosion resistance is independent of a material's hardness [20,93,94,95].

When corrosion exists, the mechanical properties of materials change. Guo *et al.* [4] investigated the degradation of the surface mechanical properties of pure iron in solutions with an applied current density of 0.5 mA/cm^2 and 1 mA/cm^2, and found that the mechanical properties are degraded by the corrosion current. Based on this, it was concluded that the decrease of erosion resistance in the process of erosion-corrosion might be due to the surface mechanical degradation caused by

corrosion current. Gutman [71] provided both experimental evidence and a theoretical analysis, and pointed out that the hardness and strength of the surface layer would decrease with the increase of the anodic dissolution current density. Lu and Luo [6] presented a theoretical prediction regarding the relationship between the additional erosion rate with the existence of a corrosion current and the degradation of surface hardness. The relation is as follows:

$$\frac{e_c}{e_0} = -n\frac{\Delta Hv}{Hv} \tag{2-7}$$

where ΔHv is the difference of hardness in the process of corrosion and the hardness without corrosion, and n is the experimental constant, which differs between erosion systems.

2.3.2 Hydrodynamic properties

2.3.2.1 Flowing velocity

The slurry is a liquid/solid two phase flow system. As opposed to the single flow system, the impingement of particles must be considered. Meng *et al.* [17] found that the impact velocity of particles is a significant parameter which determines the erosion rate, and that the velocity of impinging particles is directly

related to the slurry velocity. Postlethwaite *et al.* [96] represented the relationship of erosion-corrosion rate and flow velocity with an equation shown in **Eq. 2-8**

$$w = m_1 M_p f(\theta) U^{m_2} \tag{2-8}$$

where M_p is the weight of particles per unit volume of solution, $f(\theta)$ is the function regarding the dependence of erosion rate on impact angle, and m_1 and m_2 are constants related to the erosion-corrosion system. Some researchers also found a power law relationship between erosion-corrosion rate and flow velocity and pointed out that the value of exponents are between 1 and 4 [10,97,98]. However, some contradictions exist. Guo *et al.* [3] investigated the erosion-corrosion behaviour of AISI 1045 low carbon steel in a flowing slurry with rotating speeds of both 6000 and 9000 rpm, and found that the change of velocities in the experimental range would not influence their polarization curves. Also, Nesic *et al.* [99] pointed out that the velocity is not the best parameter for characterizing the influence of a slurry. They found that it is better to use Reynold's number or shear stress to correlate flow with erosion-corrosion.

2.3.2.2 Particle concentration

For lower particle concentrations, the erosion rate is observed to increase linearly with the particle concentration. For slurries with higher concentrations, the

erosion rate will still increase with the particle concentration, but it will rise progressively more slowly, not linearly. Hutchings [10] pointed out that this departure in higher particle concentrations is due to interference among particles. In lower particle concentrations, due to the particles' relative independence of each other, the erosion rate increases relatively linearly. He also predicted that if each particle acts independently in the slurry, the erosion rate will increase linearly with the particle concentration. He researched the material loss behaviour of mild steel in silica sand slurry, and found that in particle volume concentrations lower than 12%, the material loss would increase linearly. When a power relation is used to fit the erosion rate vs. particle concentration, the exponent is less than unity.

When corrosion exists, the situation becomes more complex. Guo *et al.* [3,43] investigated the effect of sand concentration on corrosion current density in both active and passive system. For active systems [3], she studied the concentration effect on AISI 1045 low carbon steel under different rotating speeds with sand weight concentrations of 0%, 20%, and 35%, and she found that the polarization behaviour is not dramatically changed with different sand concentrations. For passive systems [43], the sand concentration largely affected the corrosion current density, and the current density increased with the particle concentration. The fitting curve obeys a power law with exponent less than unity. Lu and Luo [100] proposed a theoretical model to illustrate the passive current responses to the slurry sand concentration, and this model gives a good fit to that relationship.

2.3.2.3 Particle property

The erosion-corrosion process is dependent on particle properties. The erosion rate strongly depends on the hardness, size, and shape of the particles involved. Hutchings [10] found that particles that are 1.2 to 1.5 times harder than the target material surface experience higher erosion rates than other particles. Oka *et al.* [101] investigated the dependence of particle size on the erosion rate of steel when impacted by quartz particles, and found that the erosion rate tends to increase up to a critical value, and the erosion rate is relatively constant above this critical value. Also, the erosion would be affected by the shape of the particles [10]. Generally speaking, more sharp and angular particles will cause a higher erosion rate.

However, the corrosion process is not as sensitive to particle properties. Stack *et al.* [31] investigated the polarization behaviour of chromium steel, and reported that there is no apparent difference created by changing the sizes of alumina particles.

2.3.2.4 Impinging angles

The erosion-corrosion rate is largely dependent on the impinging angles. Finnie [102] investigated the erosion behaviour of aluminium and its oxide in impinging angles from nearly 0° to 90°. He found that for aluminium, as a relatively soft material, the highest erosion rate occurs between 15° to 30°, while for aluminium oxide, a relatively hard material, the maximum erosion rate occurs at 90°.

He explained that this angle difference is due to the changing of erosion mechanisms from a soft material to a hard material. The erosion weight loss of soft materials is mainly caused by plowing and cutting. Weight loss of hard materials is due to fracture mechanisms, and at 90°, hard materials have the lowest facture resistance, hence the highest erosion rate.

The impinging angles will also influence the corrosion process. Burstein *et al.* [103] investigated the effect of impingement angles on corrosion current rises due to rupture/removal of oxide film on surface. He reported that at oblique angles, the current rise is greater and the rise time is longer than those at normal incidence.

2.3.3 Electrochemical parameters

2.3.3.1 pH of slurry

The pH of slurry can heavily change erosion-corrosion behaviour. As hydrogen ions are quite reactive, they can react with the metal ions relatively quickly, resulting in both more severe degradation on the surface and lower erosion resistance in acidic solutions. Guo *et al.* [104] investigated the erosion-corrosion behaviour of low carbon steel in erosive slurries with pH of 4, 7, 10, and found that the erosion rate was highest in the solution with a pH of 4 and lowest in the solution with a pH of 7, with the solution with a pH of 10 in between. Zhou *et al.* [105] studied the pH's effect on the erosion-corrosion characteristics of ductile cast iron

under an open circuit potential and found the same results. They explained that the slurry with the lower pH would result in a higher corrosion current density under an open circuit potential, hence lowering erosion resistance.

2.3.3.1 Corrosion current density

Generally speaking, the erosion rate, with the existence of corrosion, increases with corrosion current density. Lu *et al.* [6] investigated the effect of corrosion current density on the erosion-corrosion rate and found that the erosion rate (after the contribution of corrosion material loss has been deducted) increases linearly with the logarithm of the anodic current density. He also proposed an equation to theoretically calculate the corrosion-enhanced erosion rate with an anodic current density

$$\frac{e_c}{e_0} = Z \log\left(\frac{i_a}{i_{th}}\right) \tag{2-9}$$

where i_A and i_{th} are the actual anodic current density and the threshold density that causes surface mechanical degradation. Z is the constant that varies between systems. This equation indicates that the erosion rate increases linearly with the logarithm of anodic current density.

2.4 Topic selection

The review above includes various parts of material loss processes, the mechanism of the synergistic effect, and the main factors that influence the erosion-corrosion process. Existing qualitative models described the erosion-corrosion process. Some of the phenomena are still not well understood. For example, as mentioned in **Section 2.3.3.1**, the pH of a solution will influence its erosion-corrosion process. However, it only considered the difference among acid, neutral and alkaline solutions. It should be considered and studied with more specific variables, i.e. effect of increasing either the H^+ or OH^-, the effect of anions in an acid, or the effect of cations in an alkaline. Another example is that there are still not enough accurate quantitative models to evaluate the erosion-corrosion rate according to kinetic parameters.

The topics selected in this thesis are divided into two main parts:

1. As mentioned above, the erosion-corrosion rate is largely dependent on the solution composition, i.e. pH, concentration, etc. The first part investigates what specific parameters of solution composition influence the erosion-corrosion rate, i.e. H concentration, types of ions, etc.
2. Due to the lack of quantitative models to evaluate the erosion-corrosion process, the second part of this thesis developed a theoretical model to correlate the corrosion current to repassivation kinetics.

References

[1] R. Babu, S. Bhaskar, K. Chockkalingam, G.T. Parthiban, N.S. Rengaswamy, "Erosion corrosion of HSLA steel in a coal slurry", Corrosion Prevention and Control, v43, n5 (1996), pp. 131-134.

[2] M.M. Stack, B.D. Jana, "Modelling particulate erosion-corrosion in aqueous slurries: Some views on the construction of erosion-corrosion maps for a range of pure metals", Wear, v256 (2004), pp. 986-1004.

[3] H.X. Guo, B.T. Lu, J.L. Luo, "Interaction of mechanical and electrochemical factors in erosion-corrosion of carbon steel", Electrochimica Acta 51 (2005), p. 315-323.

[4] H.X. Guo, B.T. Lu, J.L. Luo, "Response of surface mechanical properties to electrochemical dissolution determined by in situ nanoindentation technique", Electrochemistry Communications, v8, pp. 1092-1098.

[5] B, T. Lu, J. L. Luo, "Prediction of Synergistic Effect in Erosion Corrosion", submitted to Corrosion Science (2007).

[6] B.T. Lu, J.L. Luo, "Synergism of electrochemical and mechanical factors in erosion - corrosion", Journal of Physical Chemistry B, (2006), pp. 4217-4231.

[7] ASTM Standard Designation G119-93: Standard Guide for Determining Synergism between Wear and Corrosion, 1993, p.139.

[8] Z. Yue, P. Zhou, J. Shi, "Some factors influencing corrosion-erosion performance of materials", Wear of Materials, ASME, New York (1987), pp. 763-768.

[9] Y. Zheng, Z. Yao, X. Wei, W. Ke, "Synergistic effect between erosion and

corrosion in acidic slurry medium", Wear 186-187 (1995), pp. 555-561.

[10] I.M. Hutchings, "The Erosion of Materials by Liquid Flow", MTI Publication No.25, Material Technology Institute of the Chemical Process Industries (1986).

[11] S.A. Bradford, Corrosion Control, p. 1

[12] D.A. Jones, Principles and Prevention of Corrosion, Upper Saddle River, USA, Prentice Hall, 1996.

[13] C.N. Cao, Principles of Electrochemical Corrosion, Beijing, China, Chemical Industry Press, 2004.

[14] J. Weber, "Flow induced corrosion: 25 years of industrial research", British Corrosion Journal 27 (3) (1992), p.193.

[15] B. Poulson, "Electrochemical Measurements in Flowing Solutions", Corrosion Science 23 (4) (1983), pp. 391-430.

[16] E. Heitz, "Chemo-mechanical effects of flow on corrosion", Corrosion 47 (2) (1991), pp.135-145

[17] H.C. Meng, K.C. Ludema, "Wear models and predictive equations: their form and content", Wear 181-183 (1995) p.443

[18] I. Finnie, in Proceeding of the Third National Congress on Applied Mechanics, New York, American society of Mechanical Engineers, 1958, p.527.

[19] I. Finnie, "Some observations on the erosion of ductile metals", Wear 19 (1972), pp. 81-90.

[20] A.V. Levy, in ASM International, Materials Park, OH, USA, 1995,

[21] P. Shewmon, G. Sundararajan, "Erosion of metals", Annual Review of Materials Science 13 (1983), pp. 301-318.

[22] J.G.A. Bitter, "A study of erosion phenomena", Wear 6 (1963), pp. 5-21

[23] G. Sundararajan, P.G. Shewmon, "A new model for the erosion of materials at normal incidence", Wear 84 (1983), p. 237.

[24] S. Endo, M. Nagae, "Comparison of experimentally measured and theoretically predicted erosion rates of steels in slurries of low velocity", ISIJ International 36 (1) (1996), pp. 87-94.

[25] I.M. Hutchings, "A model for the erosion of metals by spherical particles at normal incidence", Wear 70 (1981), pp. 269-281.

[26] M. Matsumura, Y. Oka, H. Hiura, and M. Yano, "The role of passivating film in preventing slurry erosion-corrosion austenitic stainless steel", ISIJ Int. 31 (2) (1991), p. 168-176.

[27] Y. Li, G.T. Burstein, I.M. Hutchings, "The influence of corrosion on the erosion of aluminium by aqueous silica slurries", Wear 186 (2) (1995), p. 515.

[28] M.F. Ashby, S.C. Lim, "Wear-mechanism maps", Scripta Metallurgica et Materialia 24 (5) (1990), pp. 805-810.

[29] S.C. Lim, M.F. Ashby, "WEAR-MECHANISM MAP", Acta Materialia 35 (1995), pp. 1-24.

[30] M.M. Stack, F.H. Stott, "Approach to modelling erosion-corrosion of alloys using erosion-corrosion maps", Corrosion Science 35(5-8) (1993), pp. 1027-1034.

[31] M.M. Stack, J.S. James, Q. Lu, "Erosion-corrosion of chromium steel in a rotating cylinder electrode system: Some comments on particle size effects", Wear 256 (2004), pp. 557-564.

[32] M.M. Stack, N. Corlett, S. Zhou, "Methodology for the construction of the erosion-corrosion map in aqueous environments", Wear 203-204 (1997), pp. 474-488.

[33] M.M. Stack, N. Corlett, S. Turgoose, "Some recent advances in the development of theoretical approaches for the construction of erosion-corrosion maps in aqueous conditions", Wear 233-235 (1999), pp. 535-541.

[34] M.M. Stack, N. Corlett, S. Zhou, "Impact angle effects on the transition boundaries of the aqueous erosion-corrosion map", Wear 225, 1 (1999), pp. 190-198

[35] M.M. Stack, S. Zhou, R.C. Newman, " Identification of transitions in erosion-corrosion regimes in aqueous environments", Wear 186-187 (1995), pp. 523-532.

[36] M.M. Stack, N. Pungwiwat, "Erosion-corrosion mapping of Fe in aqueous slurries: Some views on a new rationale for defining the erosion-corrosion interaction", Wear 256 (5) (2004), pp. 565-576.

[37] M.M. Stack, N. Corlett, and S. Turgoose, "Some thoughts on modeling the effects of oxygen and particle concentration on the erosion-corrosion of steels in aqueous slurries", Wear 255 (2003), pp. 225-236.

[38] W. Li, D.Y. Li, "Influence of surface morphology on corrosion and

electronic behavior", Acta Materialia 54 (2) (2006), pp. 445-452.

[39] W. Li, D.Y. Li, "On the correlation between surface roughness and work function in copper", The Journal of Chemical Physics 122 (2005)

[40] K. Sasaki, G.T. Burstein, "Generation of surface roughness during slurry erosion-corrosion and its effect on the pitting potential", Corrosion Science 38 (12) (1996), pp. 2111-2120.

[41] B.T. Lu, J.L. Luo, H.Y. Ma, "A theoretical model on electrochemical response of passivated metals to solid particle impingement", Journal of The Electrochemical Society 154 (3) (2007), pp. 159-168.

[42] X.Y. Wang, D.Y. Li, "Application of an electrochemical scratch technique to evaluate contributions of mechanical and electrochemical attacks to corrosive wear of materials", Wear 259 (2005), pp. 1490-1496.

[43] H.X. Guo, B.T. Lu, J.L. Luo, "Study on passivation and erosion-enhanced corrosion resistance by Mott-Schottky analysis", Electrochimica Acta 52 (2006), pp. 1108–1116.

[44] X.Z. Zhao, N. Cui, J.L. Luo, S. Chiovelli, "Effects of erosion on corrosion of type 430 and 316 stainless steels in aqueous environments", British Corrosion Journal 37 (1) (2002), pp. 63-68.

[45] B.W. Madsen, "Measurement of erosion–corrosion synergism with a slurry wear test apparatus", Wear 123 (1988), p. 127.

[46] D. Li, X. Mao, R. Zhu, "Kinetics of passive film formation on scratched bare surfaces of stainless steels in magnesium chloride solutions", Corrosion 49 (11) (1993), pp. 877-884.

[47] T.A. Adler, R.P. "Repassivation of 304 stainless steel investigated with a single scratch test", Walters, Corrosion 49 (5), pp. 399-408.

[48] G.T. Burstein, K. Sasaki, "Detecting electrochemical transients generated by erosion-corrosion", Electrochimica Acta 46 (2001), pp. 3675-3683.

[49] G.T. Burstein, K. Sasaki, "Birth of corrosion pits as stimulated by slurry erosion", Corrosion Science 42 (2000), pp. 841-860.

[50] C.W. Chen, B.T. Lu, J.L. Luo, in Conference of Metallurgist of CIM, Vancouver, Canada, 2003

[51] C. Duret-Thural, J.P. Audouard, L. Renard, in Innovation stainless steel, Florence, Italy, 1993

[52] S. Zhou, M.M. Stack, R.C. Newman, "Electrochemical studies of anodic dissolution of mild steel in a carbonate-bicarbonate buffer under erosion-corrosion conditions", Corrosion Science 38 (1996), pp. 1071-1084.

[53] U.K. Mudali, P. Shankar, S. Ningshen, R.K. Dayal, H.S. Khatak, B. Raj, "Effect of Strain-Induced Deformation on Corrosion Behavior of AISI 304 Stainless Steel", Corrosion Science 44 (2002), p. 2183.

[54] S. Yin, D.Y. Li, "Effects of prior cold work on corrosion and corrosive wear of copper in HNO_3 and NaCl solutions", Materials Science and Engineering A 394 (2005), p. 266.

[55] J. Li, Y.G. Zheng, J.Q. Wang, Z.M. Yao, Z. Wang, F, W. Ke, "Depassivation and repassivation of AISI321 stainless steel surface during solid particle impact in 10% H_2SO_4 solution", Wear 186-187 (1995), p. 562.

[56] M. Mayuzumi, J. Ohta, T. Arai, "Effects of cold work, sensitization

treatment, and the combination on corrosion behavior of stainless steels in nitric acid", Corrosion 54 (4) (1998), pp. 271-280.

[57] B.T. Lu, J.L. Luo, in The 2nd Environment-Induced Cracking in Materials, (EICM-2), Banff, Alberta, Canada, 2004

[58] J. Postlethwaite, "Components of erosion-corrosion in aqueous slurries of sand " Corrosion 37 (1) (1981), pp. 1-5.

[59] D. C. William, Materials science and Engineering: an introduction., 7th Edition

[60] S. Das, D.P. Mondal, R. Dasgupta, B.K. Prasad, " Mechanisms of material removal during erosion-corrosion of an Al-SiC particle composite", Wear 236 (1-2) (1999), pp. 295-302.

[61] Y.L. Saraswathi, S. Das, D.P. Mondal, "Erosion-corrosion behavior of SiC particle-reinforced Al-Si alloy in NaOH slurry", Metallurgical and Materials Transactions A 36 (8) (2005), pp. 2259-2262.

[62] M. Reyes, A. Neville, "Mechanisms of erosion-corrosion on a cobalt-base alloy and stainless-steel UNS S17400 in aggressive slurries", Journal of Materials Engineering and Performance 10 (6) (2001), pp. 723-730.

[63] D.A. Jones, A.F. Jankowski, "Anodically enhanced. diffusion in Cu/Ag thin film couples", Scripta Metallugica and Materialia, 29 (1993), p.701.

[64] D.A. Jones, A.F. Jankowski, G.A. Davidson, "Room-temperature diffusion in Cu/Ag thin-film couples caused by anodic dissolution", Metallurgical and Materials Transactions A 28 (1997), p. 843.

[65] D.A. Jones, "Localized surface plasticity during stress corrosion cracking",

Corrosion 52 (5) (1996), pp. 356-362.

[66] C.H. Caceres, B.I. Selling, "Casting defects and the tensile properties of an Al-Si-Mg alloy", Materials Science and Engineering A 220 (1996), pp. 109-116.

[67] N. Chawla, X. Deng, "Microstructure and mechanical behavior of porous sintered steels", Materials Science and Engineering A 390 (2005), p. 98.

[68] A. Hadrboletz, B. Weiss, "Fatigue behaviour of iron based sintered material: A review", International Materials Reviews 42 (1997), pp.1-44.

[69] C. Tekmen, I. Ozdemir, U. Cocen, K. Onel, "The mechanical response of Al-Si-Mg/SiC_p composite: Influence of porosity", Materials Science and Engineering A 360 (2003), pp. 365-371.

[70] P. Rehbinder, "New physico-chemical phenomena in the deformation and mechanical treatment of solids", Nature 159 (4052) (1947), pp. 866-867.

[71] E.M. Gutman, Mechanochemistry of Materials, Great Abington, Cambridge, UK, Cambridge International Science Publishing, 1998.

[72] B. Gu, W.Y. Chu, W. Chu, L.J. Qiao, C.M. Hsiao, "Effect of anodic polarization on the ambient creep of brass", Corrosion Science 36 (8) (1994), pp.1437-1445

[73] B.Q. Wang, G.Q. Geng, A.V. Levy, "Effect of microstructure on the erosion-corrosion of steels", Wear 151 (1991), pp. 351-364.

[74] L.G. Peterson, G.A. Sargent, H. Conrad, "Effect of microstructure on the erosion of steel by solid particles", Wear of Materials (1985), pp. 661-670.

[75] B.A. Lindsley, A.R. Marder, "Solid particle erosion of an Fe-Fe_3C metal

matrix composite", Metallurgical and Materials Transactions A 29 (1998), p. 1071.

[76] G. Bregliozzi, A. Di Schino, H. Haefke, J.M. Kenny, "Cavitation erosion resistance of a high nitrogen austenitic stainless steel as a function of its grain size", Journal of Materials Science Letters 22 (13) (2003), pp. 981-983.

[77] S.Y. Yu, H. Ishi, T.H. Chuang, "Corrosive wear of SiC whisker and particulate reinforced 6061 aluminum alloy composites", Metallurgy and Materials Transaction A 27 (1996), p. 2653.

[78] P.P. Trazaskoma, "Pit morphology of Al alloy and SiC/Al metal matrix composites", Corrosion 46 (1996), p. 402.

[79] B.F. Levin, J.N. DuPont, A.R. Marder, "Effect of second phase volume fraction on the erosion resistance of metal-matrix composites", Wear 238 (2) (2000), pp. 160-167.

[80] E.J. Wentzel, C. Allen, "Erosion-corrosion resistance of tungsten carbide hard metals with different binder compositions", Wear 181 (1995), pp. 63-69.

[81] K. Ghosh, T. Troczynski, A.C.D. Chaklader, "Aluminum-silicon carbide coatings by plasma spraying", Journal of Thermal Spray Technology 7 (1) (1998), pp. 78-86.

[82] V.A. Pugsley, C. Allen, "Microstructure/property relationships in the cavitation erosion of tungsten carbide-cobalt", Wear, 233-235 (1999), pp. 93-103.

[83] B.W. Madsen, in Proceedings of the International Conference on the Wear of Materials", Wear of Materials (1985), p. 345.

[84] G.M.C. Lee, "Erosion resistance of plain carbon steels under water droplet impact conditions", Wear 141 (1) (1990), pp. 185-201.

[85] J.D. Majumdar, I. Manna, "Laser surface alloying of AISI 304-stainless steel with molybdenum for improvement in pitting and erosion-corrosion resistance", Materials Science and Engineering A 267 (1999), pp. 50-59.

[86] D.J. Mills, R.D. Knutsen, "Investigation of the tribological behaviour of a high-nitrogen Cr-Mn austenitic stainless steel", Wear 215 (1998), pp. 83-90.

[87] A. Toro, A. Sinatora, D.K. Tanaka, A.P. Tschiptschin, "Corrosion-erosion of nitrogen bearing martensitic stainless steels in seawater-quartz slurry", Wear 251 (2001), pp. 1257-1264.

[88] H.M. Jing, X.Q. Wu, Y.G. Zheng, Z.M. Yao, W. Ke, "Effect of Mo content on the corrosion and erosion-corrosion of stainless steel in oil containing naphthenic acid", Acta Metallurgica Sinica 38 (10) (2002), pp. 1067-1073.

[89] W.A. Metwally, M.K. Samy, "Evaluation of abrasive-wear and erosion-corrosion resistance of high-Cr cast-steel", Steel Research 65 (10) (1994), pp. 455-458.

[90] B.T. Lu, J.L. Luo, S. Chiovelli, "Corrosion and wear resistance of chrome white irons - A correlation to their composition and microstructure", Metallurgical and Material Transactions A (37) (2006), pp. 3029-3038.

[91] G.L. Sheldon, A. Kanhere, "An investigation of impingement erosion using single particles", Wear 21 (1972), pp. 195-209.

[92] Y.I. Oka, M. Matsumura, T. Kawabata, "Relationship between surface hardness and erosion damage caused by solid particle impact", Wear 162-164

(1993), pp. 688-695.

[93] A. Neville and X. Hu, "Mechanical and electrochemical interactions during liquid-solid impingement on high-alloy stainless steels", Wear 250-251 (2001), pp. 1284-1294.

[94] A. Levy, G. Hickey, "Erosion of corrosion-resistant surface treatments on alloy steels", Wear 108 (1986), p. 61-79.

[95] U. Malayoglu, A. Neville, "Mo and W as alloying elements in Co-based alloys - Their effects on erosion-corrosion resistance", Wear 259 (1-6) (2005), pp. 219-229.

[96] J. Postlethwaite, M.H. Dobbin, K. Bergevin, "The mechanism of erosion-corrosion in slurry pipelines", Materials Science Forum 8 (1985), pp. 13-22.

[97] A.V. Levy, P. Yau, "Erosion of steels in liquid slurries", Wear 98 (1-3) (1984), pp. 163-182.

[98] A.V. levy, N. Jee, P. Yau, "Erosion of steels in coal-solvent slurries", Wear 117 (2) (1987), pp. 115-127.

[99] S. Nesic, J. Postlethwaite, "Hydrodynamics of disturbed flow and erosion-corrosion. Part I. Single-phase flow study", Canadian Journal of Chemical Engineering 69 (1991), pp. 698-703.

[100] B.T. Lu and J.L. Luo, in The 16th International Corrosion Congress, Beijing, China, 2005, Sept 19-24, Paper No. 12.

[101] Y. Oka, M. Matsumura, "Erosive wear testing apparatus-simulation of erosion caused by slurry of low impingement velocity", Wear of Materials

(1983), pp. 360-366.

[102] I. Finnie, J. Wolak, Y. Kabil, "Erosion of metals by solid particles", Journal of Materials 2 (3) (1967), pp. 682-700.

[103] G.T. Burstein, K. Sasaki, "Effect of impact angle on the slurry erosion-corrosion of 304L stainless steel", Wear 240 (2000), pp. 80-94.

[104] H.X. Guo, B.T. Lu, J.L. Luo, "Non-Faraday material loss in flowing corrosive solution", Electrochimica Acta 51 (2006), pp. 5341-5348

[105] Y.X. Zhou, Z.L. Lu, M. Zhan, "An investigation of the erosion–corrosion characteristics of ductile cast iron", Materials and Design 28 (2007), pp. 260-265.

Chapter 3

Experimental Apparatus and Procedures

3.1 Materials

In the electrochemical and erosion-corrosion tests, carbon steel AISI 1018 (A1018) and AISI 1045 (A1045) were used (as received). Their nominal compositions are listed in **Table 3-1**. The nanoindentation test was carried out on pure iron to avoid disturbance from the phase composition and alloy elements. The composition of commercial pure iron is listed in **Table 3-2**. The microstructures of A1018, A1045 and pure iron are shown in **Fig. 3-1**.

Table 3-1 Chemical composition of A1018 and A1045 steels (wt%)

Steel	C	Mn	P	S	Si	Fe
AISI 1018	0.15-0.20	0.30-0.60	0.030	0.035	-	Balance
AISI 1045	0.43-0.50	0.60-0.90	0.030	0.035	0.35	Balance

In erosion-corrosion tests, the sand was unground sand with a diameter of 200μm-300μm, which is commercially available from the U.S. Silica Company,

Ottawa. An SEM picture of the sand is presented in **Fig. 3-2**. Its main chemical composition and mechanical properties are listed in **Table 3-3**.

Table 3-2 Chemical composition of commercial pure iron (wt%)

C	Mn	P	Si	Cr	Al	B	Fe
0.003	0.12	0.006	0.01	0.01	0.32	0.009	Balance

Table 3-3 Chemical composition and mechanical properties of sand

Chemical	Size (mesh)	Diameter (μm)	Spe. Gravity (g/cm3)
99.7 SiO2	50-70	200-300	2.65

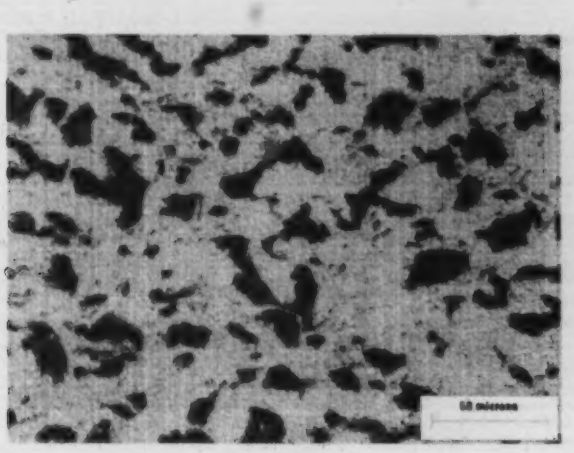

(a)

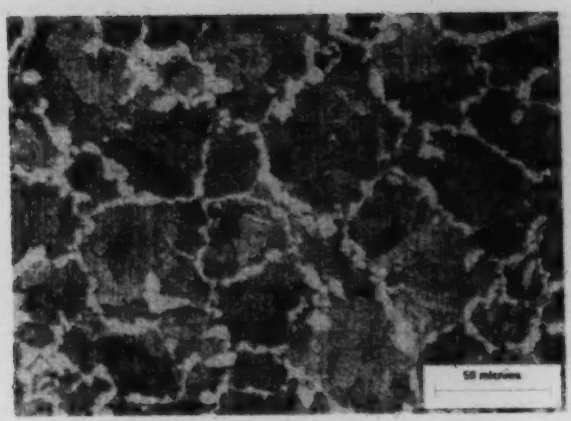

(b)

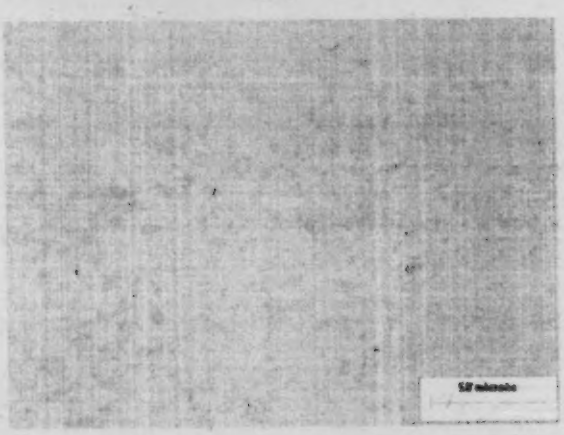

(c)

Figure 3-1 Microstructures of (a) A1018, (b) A1045 and (c) pure iron

Figure 3-2 Silica sand by SEM

3.2 Experimental Setup and Procedures

In order to investigate erosion-corrosion problems, several equipments were used in this work: a) a rotating cylinder electrode **(RCE)** system; b) a scratch system and c) a nanoindentation system.

3.2.1 Rotating cylinder electrode system

3.2.1.1 System description

In the RCE system, the specimen used, shown in **Fig. 3-3,** is a steel toroid, 8 mm in height and 25 mm in diameter with a hole for mounting the specimen.

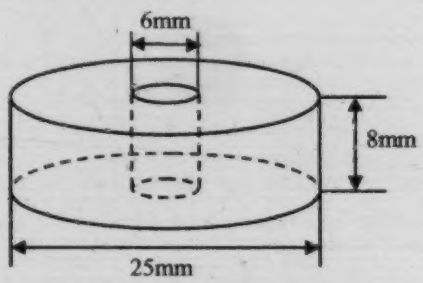

Figure 3-3 Steel specimen for RCE system

Fig. 3-4 shows the RCE system for the erosion-corrosion tests. An AFMSRX rotator **(Pine instrument Company, PA, USA)** was applied to drive the steel specimen in the slurries. The velocity range of the rotator is from 0 to 10,000 rpm. The test specimen was mounted on the rotating shaft, which is made of stainless

steel. Polytetrafluoroethylene (**PTFE**) wafers and rubber plates were placed on the bottom and top of the specimen to avoid crevice corrosion. In the rotating cell, the counter electrode was a platinum wire, placed on the bottom of the cell. Four baffles, mounted at 90° from each other on the side of the electrochemical cell, were used to minimize vortex formation and axial flow in the slurry. A saturated calomel electrode (**SCE**) was used as a reference electrode. The reference electrode was connected to the cell with an agar tunnel tip. The agar tip acted as a salt bridge and prevented possible mingling action of the electrolytes. Solartron electrochemical measurement (**Solartron Instruments**) equipment was connected to the 3-electrode rotating system to control the electrochemical parameters.

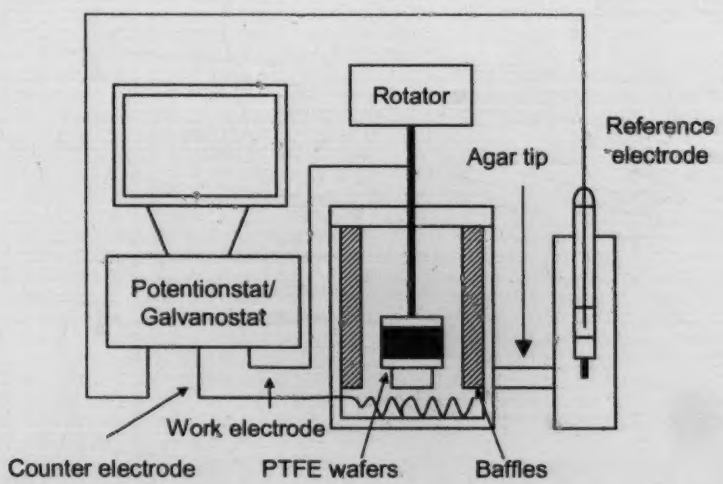

Figure 3-4 Schematic set-up of rotating system for erosion-corrosion tests

3.2.1.2 Experimental procedure

Before any tests were carried out, the electronic contact was checked by a multimeter to ensure good contact between the rotating shaft and the interval hole of the specimen. Also, the rotating speed was calibrated by a tachometer to ensure a stable rotating speed in all of the tests.

In the RCE system, erosion-corrosion weight loss and polarization curves were measured. Before the tests were carried out, the work surface of the specimen was ground with silica carbide abrasive sand paper to 600 grit. The work surface of the specimen was cleaned according to ASTM Standard G1-90 [1]. The specimen was mounted on the rotating shaft and was then immersed into the slurries. During this process, specific electrochemical conditions, i.e. fixed potential, fixed current density, and dynamic polarization condition, were applied to the specimen. The rotating speed for all tests were 9000 rpm, and the weight loss test lasted 30 min. After the tests, the work surface was cleaned with a solution of hydrochloric acid with hexamethylene tetramine acting as the inhibitor. The weight was measured before and after the erosion-corrosion tests by an analytical balance (**Scientech, SA510**) with the precision of 0.1 mg, the difference of weight represented the weight loss data.

3.2.1.3 Analysis of erosion-corrosion weight loss

In **Chapter 2, Eq.2-4** defined the relationship between erosion and corrosion

as follows:

$$w = e + c = e_0 + e_c + c_0 + c_e \tag{2-4}$$

Each part of the total erosion-corrosion can be determined individually by carrying out the material loss tests under different conditions as follows [2]:

(a) The total weight loss w is the difference of material weight before and after the erosion-corrosion test.

(b) The pure erosion material loss rate e_0 can be determined under cathodic protection condition, i.e. -0.85V (v.s. SCE). In this condition, the corrosion reaction between the solution and the work surface is inhibited by the applied cathodic protection, and the resulting weight loss could therefore be considered as material loss rate caused solely by a mechanical effect.

(c) The corrosion material loss rate c can be calculated by using Faraday's Second Law when the corrosion current density is known. The corrosion current density can be determined using the extrapolation method on the polarization curves. Because c is the sum of c_0 and c_e, by subtracting e_0, c_0 and c_e from w, c_e can be determined.

3.2.2 Electrode scratch system

3.2.2.1 System description

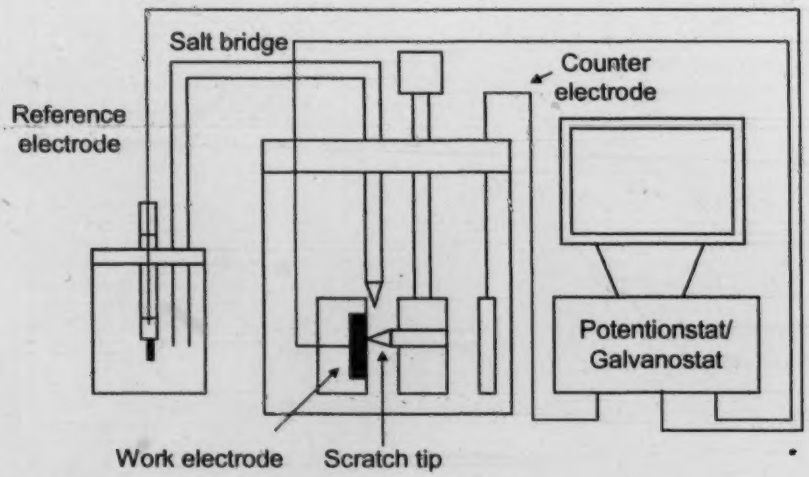

Figure 3-5 Schematic set-up of electrode scratch system

The electrode scratch system was used to investigate the breakdown and repassivation behaviour of surface oxide films. The system is shown as **Fig. 3-5**. This system is again a 3-electrode system. The computer with Solartron electrochemical measurement equipment is used to control the electrochemical parameters, i.e. control potential and record current density response. The scratch tip is placed parallel to the surface of the work electrode to make a scratch. The tip is made of alumina. Electrode scratch tests were performed to simulate the effect of sand impingement on the breakdown and repassivation process of the passive film

in a passivated erosion-corrosion system.

3.2.2.2 Experimental procedure

Before any scratch test was carried out, the specimen was grounded with silica carbide sand paper up to 1200 grit, and polished by aluminium oxide polish powder up to 0.05μm (roughness). Then the specimen was placed into an ultrasonic bath for surface debris cleaning, and the specimen was cleaned by ASTM Standard G1-90 [1]. After the specimen treatment was done, it was mounted on the scratch device and was immersed into the 3-electrode cell. Each specimen was passivated for 30 minutes at a defined passive potential. When the current was stabilized, the work surface was scratched by the alumina tip. During the test, the current response was recorded by the Solartron equipment. By analyzing the current response curve, the electrochemical behaviour and properties of the surface oxide film were compared.

3.2.3 Nanoindentation system

3.2.3.1 System description

As pointed out by many researchers [3,4,5,6,7,8] the anodic dissolution process can degrade the mechanical properties of materials, such as hardness and erosion resistance. Also, during the corrosion process, the anodic dissolution only happens on a very thin surface layer of the material [4,7]. As nanoindentation could

indent into the surface by several tens of nano-meters, it provides a good approach to investigate the surface mechanical properties during the corrosion process.

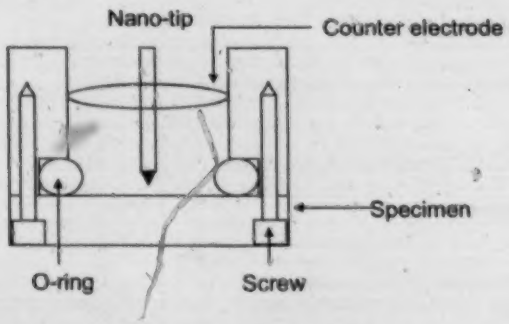

Figure 3-6 Schematic set-up of indent cell for *in-situ* nanoindentation

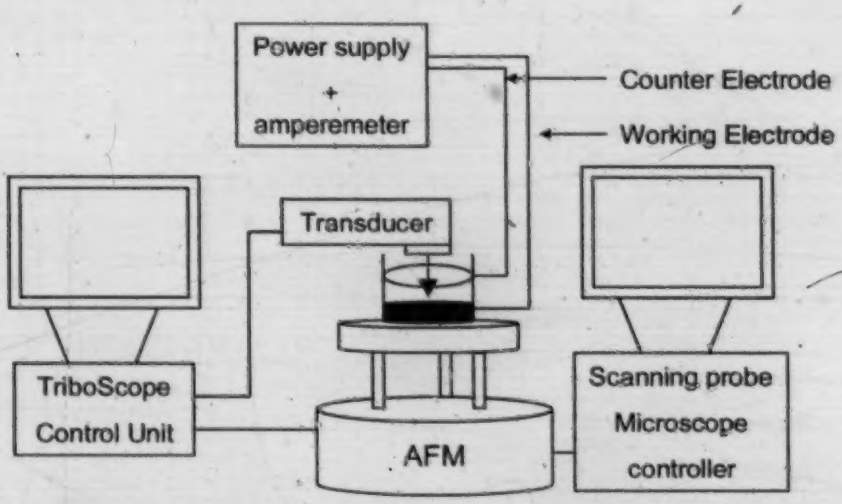

Figure 3-7 Schematic set-up of *in-situ* nanoindentation system

To investigate the mechanical properties of a passive film during electrochemical processes, Seo and Chiba [9,10,11] developed a small cell for in-situ nanoindentation. In this work, a similar cell was used as shown in **Fig. 3-6**.

The nanoindentation technique and electrochemical measurement were combined, making it possible to investigate the instantaneous response of surface mechanical properties during electrochemical dissolution. The cell was placed on the specimen and was secured with screws. The O-ring is to prevent leakage of the solution. The counter electrode is made of platinum wire, and the work electrode is a pure iron specimen.

Fig. 3-7 shows the set-up for the *in-situ* nanoindentation system. This system is placed on the stage of an Atomic Force Microscope (AFM).There are two computers to control the system: a Triboscope control unit and a scanning probe microscope controller. The former is for making the indent and analyzing the indent curve; the latter is for controlling the positioning and scanning the surface morphologies. The power supply and amperemeter are used to apply and control an applied current density. The nano-tip is mounted on the transducer to execute the indent and positioning of the tip.

3.2.3.2 Experimental procedure

The specimen for the nanoindentation was commercial pure iron. Before tests, the specimens were ground to 1200 grit, and polished by 0.05 μm aluminium oxide powder. Then, the polished specimen was put into ultrasonic cleaning equipment for surface cleaning. The specimen was cleaned according to ASTM G1-90 [1].

Before any indent was made, three calibrations were conducted: Advanced

z-axis calibration and tip area function calibration. The indent tip was controlled by electrostatic force transducer [12]. When turning on the equipment, there was sudden electrostatic impulse on the transducer and this effect made the indent displacement less accurate. The first calibration was to eliminate the effect of electrostatic impulse and ensure the accurate displacement of the indent tip. The nano-tip's shape is like that of an inverted pyramid.

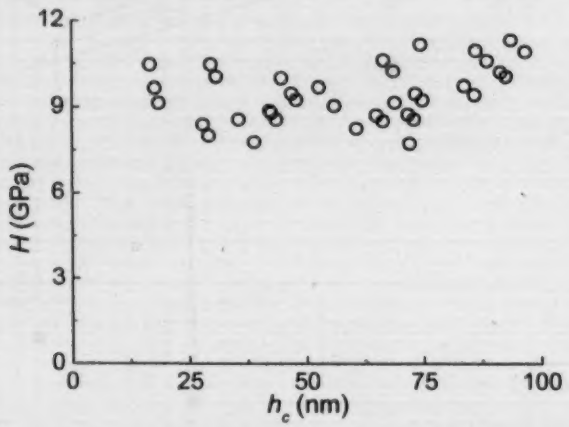

Figure 3-8 Hardness of quartz with increasing of contact depth

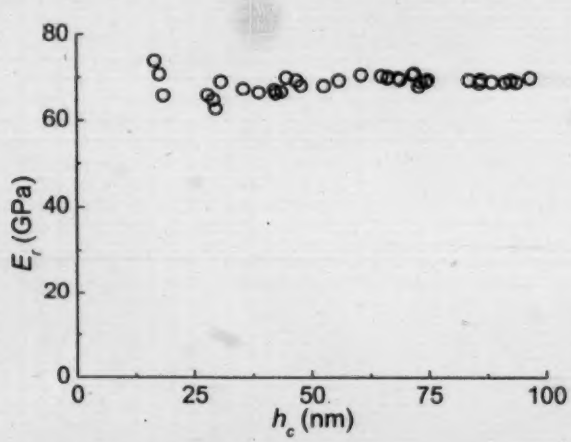

Figure 3-9 Reduced modulus of quartz with increasing of contact depth

After a series of indent tests, the nano-tip might be changed, i.e. become blunt. Under the same indent load, a blunter tip shape would make the indent shallower hence giving it a smaller area. The tested mechanical properties on the same sample might get varying results due to the shape change of tip. The second calibration is made on a standard sample (fused quartz) to eliminate this kind of effect and to stabilize the mechanical properties of the materials. **Fig. 3-8** and **Fig. 3-9** are the standardized hardness and reduced modulus data of fused quartz, respectively. The theoretical value of hardness and reduced modulus for fused quartz are 10 GPa and 69.6 GPa respectively [12].

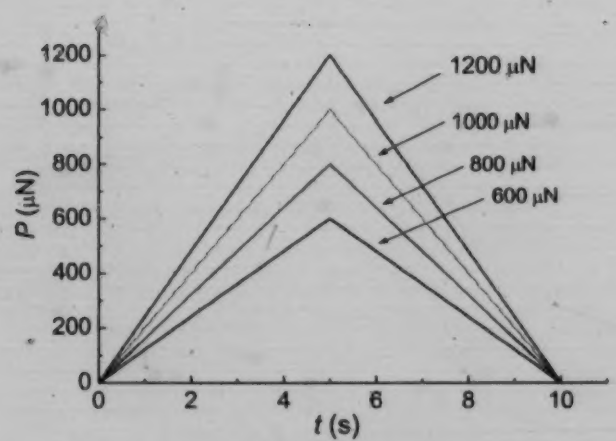

Figure 3-10 Indent load curves

After the calibrations, the nanoindentation tests could be carried out. The hardness was tested under different loads, ranging from 600μN to 1200μN.

Fig. 3-10 shows the typical indent curves obtained. The load and unload time were both 5 seconds and the maximum indent loads were from 600μN to 1200μN. After the indent was completed, an indent curve could be acquired. The surface hardness and reduced modulus were determined by analyzing the indent curve.

The nano-scratch tests could be carried out with the same set-up. **Fig. 3-11** and **Fig. 3-12** show the typical scratch load curve and lateral displacement curve. While the scratch tests were carried out on the surface of the specimen, the indent force was controlled by the specific desired function, and the lateral force was measured by a nanoindentation system. Then, the friction coefficient was determined by the ratio of lateral force and indent force.

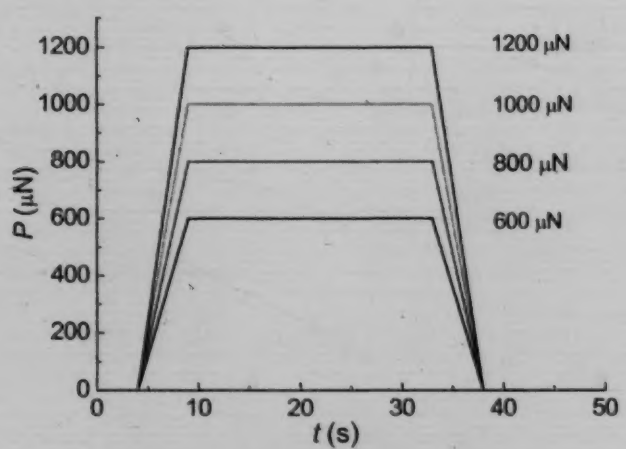

Figure 3-11 Scratch load curves

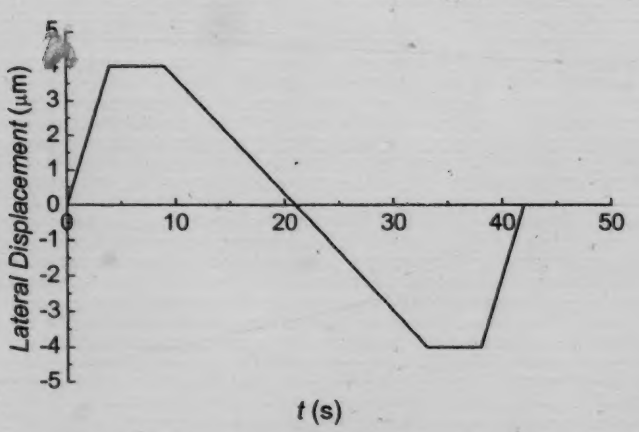

Figure 3-12 Lateral displacement of scratch tests

3.2.3.3 Calculation of surface hardness and reduced modulus

Nanoindentation mechanical property measurements are similar to conventional mechanical testing systems. For the nanoindentation process, a sharp diamond tip was indented and unloaded from the surface of the specimen. The load and displacement were recorded by the system. Mechanical properties were determined using the load and displacement curves.

Oliver and Pharr developed the analysis method [13,14]. This method has been widely used. The hardness, H, is defined as: [15]

$$H = \frac{P_{max}}{A_s} \tag{3-1}$$

where P_{max} is the maximum applied load, and A_s is the contact area made by the

indent tip. The reduced modulus, E_r, is defined as [13]:

$$E_r = \frac{\sqrt{\pi}}{2\sqrt{A_s}} S \tag{3-2}$$

S is the calculated stiffness of the target material at the peak load.

From **Eq. 3-1** and **Eq. 3-2**, the contact area A and stiffness S need to be determined before H, E_r. A_s and S can be determined from the load-depth curve, as shown in **Fig. 3-13**.

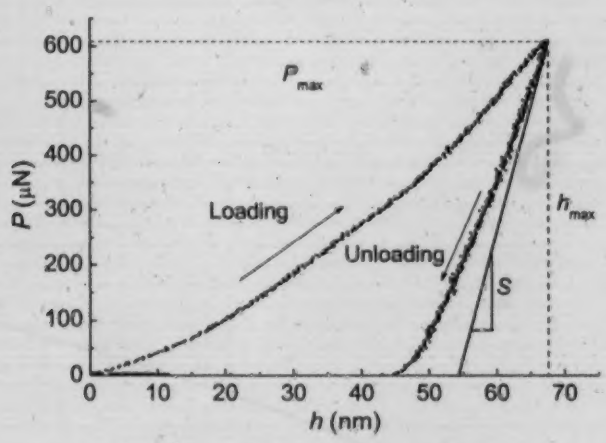

Figure 3-13 Typical load depth curve

Firstly, fit the unload curve as the form: [12]

$$P = B(h - h_f)^m \tag{3-3}$$

where B, h_f, and m are arbitrary fitting parameters. Then, the stiffness can be calculated from the derivative of **Eq. 3-3** at h_{max}: [12]

$$S = \frac{dP}{dh}(h_{max}) = mB(h_{max} - h_f)^{m-1} \tag{3-4}$$

Assuming that the tip is ideal for all of the tests, the contact area can be calculated by the corrected area function [14]:

$$A(h_c) = C_0 h_c^2 + C_1 h_c + C_2 h_c^{1/2} + C_3 h_c^{1/4} + C_4 h_c^{1/8} + C_5 h_c^{1/16} \tag{3-5}$$

C_0 is related to the tip shape. In present work, C_0 is 2.598. C_1 to C_5 are determined by the area function calibration indents on fused quartz. h_c is the contact depth, which is related to the geometric shape of the indent tip. It can be treated as the indent depth primarily caused by permanent plastic deformation. And h_c is the corrected data from h_{max}. Their relationship is as follows: [14]

$$h_c = h_{max} - \varepsilon \frac{P_{max}}{S} \tag{3-6}$$

ε is the geometric constant and it is related the shape of the tip. In present work, ε was 0.75.

A_s and S can be calculated using **Eq. 3-4** and **Eq. 3-5**. Put values A_s and S into **Eq. 3-1** and **Eq. 3-2**, and H and E_r can be acquired.

Compared to the conventional mechanical test system, there are two major advantages for the nanoindentation system. Firstly, as nanoindentation has a smaller deformation scale and displacement scale, it is more suitable to investigate the very thin surface of bulk materials. For example, it could be used to study the influence of corrosion current on surface degradation, and also to study the oxide film of passivation. Secondly, not only hardness, but many other parameters can be tested by nanoindentation, i.e. reduced modulus, indent depth, stiffness, and surface morphologies. As nanoindentation can investigate the surface mechanical properties on a very small scale, always micro and nano scale, it is widely used to study very thin surface film [16]. Also, it could be used to investigate the change of very thin surface mechanical properties. By taking these advantages, Seo and Chiba [9,10] investigate the mechanical properties of passive films in solution formed on metallic material at different potentials during the film forming process.

References

[1] ASTM Standard Designation G1-90: Standard practice for preparing, cleaning, and evaluating corrosion test specimens, 1994, p.9.

[2] ASTM Standard Designation: G119-93, Standard Guide for Determining

Synergism Between Wear and Corrosion, 1993, p.139.

[3] E.M. Gutman, Mechanochemistry of Materials, Cambridge International Science Publishing, Great Abington, Cambridge, UK (1998)

[4] S. Yin, D.Y. Li, "Effects of prior cold work on corrosion and corrosive wear of copper in HNO3 and NaCl solutions", Materials Science and Engineering A 394 (2005), p. 266.

[5] J.H. Xie, A.T. Alpas, D.O. Northwood, "Mechano-electrochemical effect between erosion and corrosion", Journal of Materials Science 38, 24 (2003), pp. 4849-4856.

[6] H.X. Guo, B.T. Lu, J.L. Luo, "Interaction of mechanical and electrochemical factors in erosion-corrosion of carbon steel", Electrochimica Acta 51 (2005), p. 315-323.

[7] B. Gu, W.Y. Chu, W. Chu, L.J. Qiao, C.M. Hsiao, "Effect of anodic polarization on the ambient creep of brass", Corrosion Science 36 (8) (1994), pp.1437-1445

[8] S. Yin, D.Y. Li, "A New Phenomenon Observed in Determining the Wear-Corrosion Synergy during a Corrosive Sliding Wear Test", Tribology Letter 29, 1 (2008), pp. 45-52.

[9] M. Chiba, M. Seo, "Effects of dichromate treatment on mechanical properties of passivated single crystal iron (100) and (110) surfaces", Corrosion Science 44 (10) (2002), pp. 2379-2391.

[10] M. Seo, M. Chiba, "Nano-mechano-electrochemistry of passive metal surfaces", Electrochimica Acta 47 (1–2) (2001), pp. 319-235.

[11] M. Seo, M. Chiba, K. Suzuki, "Nano-mechano-electrochemistry of the iron (100) surface in solution", Journal of Electroanalytical Chemistry 473 (1–2) (1999), pp. 49-53.

[12] TriboScope User Manual

[13] W.C. Oliver and G.M. Pharr, "Improved technique for determining hardness and elastic modulus using load and displacement sensing indentation experiments", Journal of Materials Research 7 (6) (1992), pp. 1564-1580.

[14] W.C. Oliver and G.M. Pharr, "Measurement of hardness and elastic modulus by instrumented indentation: Advances in understanding and refinements to methodology", Journal of Materials Research 19 (1) (2004), pp. 3-20.

[15] W.D. Callister, Materials science and engineering: an introduction, 1994.

[16] W.D. Nix, "Elastic and plastic properties of thin films on substrates: Nanoindentation techniques", Materials Science and Engineering A 234 (1997), p. 37.

Chapter 4

The Effect of Solution Composition on Erosion-Corrosion and Surface Mechanical Properties of Fe Based Alloys and Iron

4.1 Introduction

Many researchers have investigated the effect of solution compositions on the erosion-corrosion behaviour of materials [1,2,3,4,5]. They found that erosion-corrosion behaviour is largely dependent on solution compositions. In present work, the effect of solution composition on both erosion resistance and surface mechanical degradation was investigated under the galvanostatic condition. The surface mechanical properties, i.e. surface hardness and contact depth, were obtained by using in-situ nanoindentation in solutions with different compositions under the same galvanostatic control. The objective of this research was to find out how solution composition influences the erosion-corrosion process and surface mechanical properties.

4.2 Experimental details

For testing the erosion-corrosion, the experiments were carried out on AISI 1018 low carbon steel. The solution compositions are listed in **Table 4-1** and

Table 4-2. The experiments using the solutions listed in **Table 4-1** were conducted at current densities ranging from 5×10^{-4} A/cm^2 to 2×10^{-2} A/cm^2. For the solutions listed in **Table 4-2**, the applied current density was fixed at 1×10^{-3} A/cm^2. The indents were carried out 5 times in air and under cathodic protection conditions, and 3 times under anodic dissolution conditions.

Table 4-1 Solution compositions

Solution	No.	Composition
Neutral	N1	0.01M Na_2SO_4
	N2	0.1M Na_2SO_4
	N3	0.02M NaCl+0.1MNa_2SO_4
Alkaline	B1	0.02M NaOH
	B2	0.02M NaOH+0.1MNa_2SO_4
Acidic	A1	0.01M H_2SO_4
	A2	0.01M H_2SO_4+0.1MNa_2SO_4
	A3	0.02M HCl
	A4	0.02M HCl+0.02NaCl

For *in-situ* nanoindentation test, the solutions used were N2, B2, A1, A2, and A3, shown in **Table 4-1**, with an applied current density of 1×10^{-3} A/cm^2. The nano-scratch tests were carried out in solutions N2 and A2. **Fig. 4-1** shows a typical AFM image obtained in air when the peak load was 1200 μN. The crater produced by the indentation is an equilateral triangle about 0.6 μm in length, which is much smaller than the average grain size (>50 μm) of the iron sample. By applying different loads, one can obtain information regarding load and

contact depth. **Fig. 4-2** shows the typical indent curves for the tests on pure iron in air. By analyzing these curves, the contact depth (h_c) and surface hardness (H) can be acquired, as shown in **Fig. 4-3** and **Fig. 4-4** respectively. The decreasing hardness as the applied load increases is due to the volume effect. Similar results have been reported for single crystal copper and silver [6,7] and this phenomenon is known as the indentation size effect [8,9,10]

Table 4-2 Acidic solution compositions

Group A	**Group B**	**Negative Charge Concentration (mol e/l)**
0.005M H_2SO_4	0.005M H_2SO_4	0.01
0.01M H_2SO_4	0.005M H_2SO_4 + 0.005M Na_2SO_4	0.02
0.02M H_2SO_4	0.005M H_2SO_4 + 0.015M Na_2SO_4	0.04
0.05M H_2SO_4	0.005M H_2SO_4 + 0.045M Na_2SO_4	0.1
0.1 M H_2SO_4	0.005M H_2SO_4 + 0.09M Na_2SO_4	0.2
-	0.005M H_2SO_4 + 0.5M Na_2SO_4	1.01
-	0.005M H_2SO_4 +1M Na_2SO_4	2.01
Group C	**Group D**	
0.01M HCl	0.01M HCl	0.01
0.02M HCl	0.01M HCl+0.01M NaCl	0.02
0.04M HCl	0.01M HCl+0.03M NaCl	0.04
0.1 M HCl	0.01M HCl+0.09M NaCl	0.1
0.2 M HCl	0.01M HCl+0.19M NaCl	0.2
-	0.01M HCl+1M NaCl	1.01
-	0.01M HCl+2M NaCl	2.01

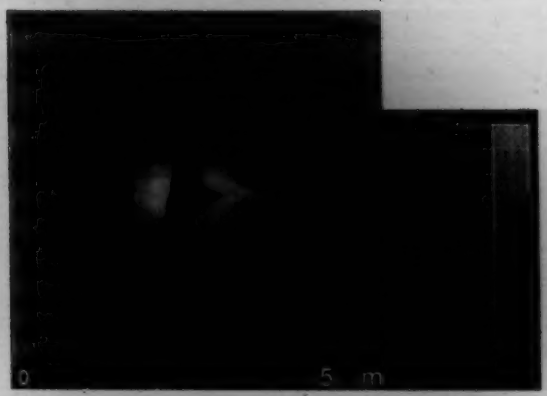

Figure 4-1 Typical AFM image obtained in air, P = 1200 μN

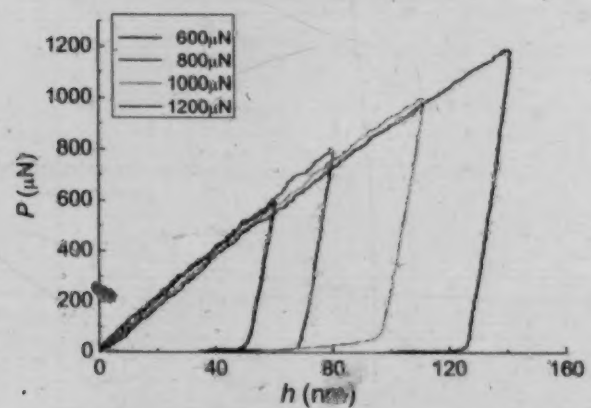

Figure 4-2 Load-depth curves of pure iron in air

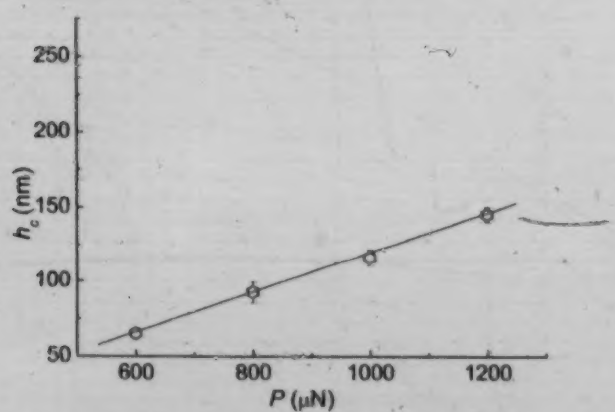

Figure 4-3 Contact depth with increasing load

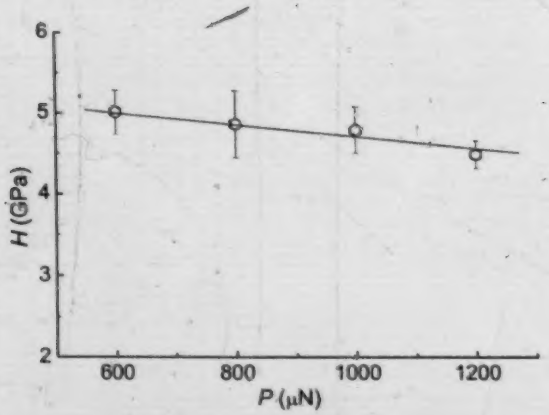

Figure 4-4 Surface hardness with increasing load

4.3 Results

4.3.1 Erosion-Corrosion Material Loss Test

The total erosion-corrosion rate with increasing applied current densities is shown in **Fig. 4-5**. It can be seen that the total erosion-corrosion rate is a linear function of the applied current densities. The data is separated into two groups; one is from using acid solutions and the other is from both neutral and alkaline solutions. Under the same applied current densities and hydrodynamic conditions, the total erosion-corrosion rate in acid is higher than that in neutral or alkaline solutions. The corrosion material loss can be calculated using Faraday's second law. By subtracting the material loss caused by corrosion from the total weight loss, the erosion rate in solutions with different compositions is found, and is shown in **Fig. 4-6**. The erosion rate is increasing with logarithm of

anodic current densities.

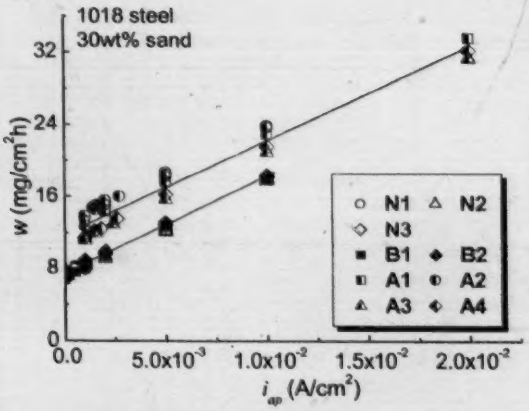

Figure 4-5 Erosion-corrosion rates with increasing of applied current densities

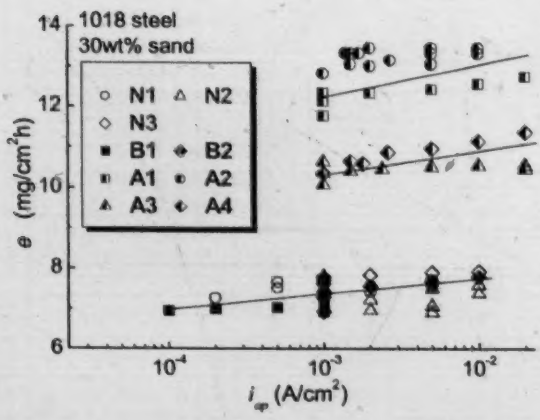

Figure 4-6 Erosion rates with increasing of applied current densities

It is clearly shown that in neutral and alkaline solutions, the erosion rates were nearly the same. This implies that the erosion rate is independent of solution composition in neutral and alkaline solutions. To further confirm this

phenomenon, more tests were carried out in neutral and alkaline solutions under both cathodic protection condition (-0.9VSCE) and anodic dissolution condition (1 mA/cm2), listed in **Table 4-3** and **Table 4-4** respectively. **Table 4-3** and **Table 4-4** clearly show that the erosion or erosion-corrosion rates in neutral and alkaline solutions are independent of solution compositions under both cathodic protection and anodic dissolution condition.

The results in **Fig. 4-6** also show that the erosion rates in acid solutions are much higher than those in neutral and alkaline solutions. Another important phenomenon is that in acid solutions with different anions, i.e. Cl^- vs. SO_4^{2-}, the erosion rates were substantially different. As the hydrogen concentration was kept unchanged (0.02M/L), the difference might have been caused by the influence of the anions (Cl^- vs. SO_4^{2-}).

Table 4-3 Weight loss under cathodic protection (-0.9V_{SCE})

Neutral	**Weight Loss Rate ($mg/cm^2/h$)**
0.1M Na_2SO_4	7.2771 ± 0.3828
1M Na_2SO_4	7.2134 ± 0.3378
Alkaline	**Weight Loss Rate ($mg/cm^2/h$)**
0.02M NaOH	7.4682 ± 0.1576
0.02M NaOH+0.1M Na_2SO_4	7.4204 ± 0.2297
0.02M NaOH+0.5M Na_2SO_4	7.2134 ± 0.3378
0.02M NaOH+1M Na_2SO_4	7.2134 ± 0.2702

Table 4-4 Weight loss under anodic dissolution (i_{ap} = 1 mA/cm^2)

Neutral	**Weight Loss Rate (mg/cm^2/h)**
0.1M Na_2SO_4	8.6465 ± 0.3828
1M Na_2SO_4	8.2882 ± 0.3378
Alkaline	**Weight Loss Rate (mg/cm^2/h)**
0.02M NaOH	8.1369 ± 0.2477
0.02M NaOH+0.1M Na_2SO_4	8.1688 ± 0.2027
0.02M NaOH+0.5M Na_2SO_4	8.2404 ± 0.3716
0.02M NaOH+1M Na_2SO_4	8.3970 ± 0.4833

Table 4-5 pH values of Group A and Group C

Negative Charge Concentration (mol e/l)	**Group A**	**Group C**
0.01	2.14	2.17
0.02	1.80	1.85
0.04	1.46	1.43
0.1	1.05	1.06
0.2	0.73	0.75

To further investigate the influence of anions, the weight loss test was used, under the same galvanostatic control (applied current density = 1 mA/cm^2) as in solution compositions listed in **Table 4-2**. In each group, the solution concentrations were increased from top to bottom. By comparing **Group A** and **Group C**, two phenomena can be investigated: a) whether the total concentration of solution will influence erosion resistance; and b) under the

same solution concentration, whether the different anions will influence the erosion resistance. As listed in **Table 4-2**, the difference between **Group A** and **Group C** and between **Group B** and **Group D** is using Na^+ partly instead of H^+ in order to investigate whether H^+ concentration will influence erosion resistance under the same solution concentration. The anion strength is the term used to determine the charge concentration of anions. The erosion rate data is obtained by subtracting the corrosion weight loss from the total erosion-corrosion rate shown in **Fig. 4-7**. These results clearly show that for solutions with the same kind of anions and under the same anodic current density, the erosion rate is independent of hydrogen concentration and anion concentration. Still, obvious erosion rate differences were observed between the groups with Cl^- and the groups with SO_4^{2-}.

The pH values of **Group A** and **Group C** were also tested as shown in **Table 4-5**. This indicates that the incomplete ionization of HSO_4^- is not the reason for the erosion rate differences between Cl- and SO_4^{2-}.

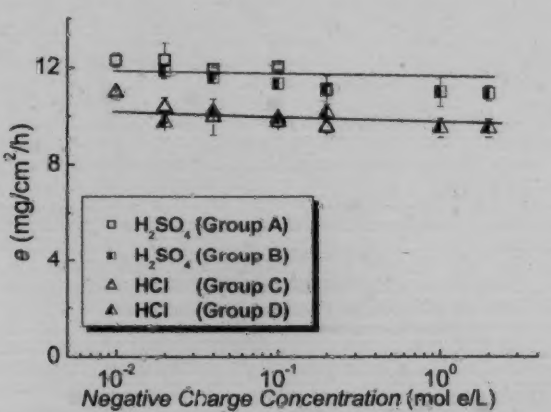

Figure 4-7 Erosion rates with increasing of negative charge concentration

4.3.2 *In-situ* nanoindentation tests

As pointed out by many researchers, corrosion can degrade the mechanical properties of materials by anodic dissolution [11,12,13,14,15,16]. It is important to investigate the surface mechanical properties during the erosion-corrosion process. Since corrosion only affects the very thin surface layer of a metal, it is reasonable to predict that the degradation of surface mechanical properties happens in this thin surface layer. Due to the indent depth in present work being always within tens of nanometers, nanoindentation is suitable for mechanical measurements on very thin surface layers.

Several typical neutral (N2), alkaline (B2), and acid solutions (A1, A2, and A3) from **Table 4-1** were chosen for this test. The contact depth and surface hardness data under cathodic protection in different solutions are displayed in **Fig. 4-8** and **Fig. 4-9**. The data in air are comparable to those under cathodic protection in alkaline and neutral solutions. It clearly shows that the cathodic current did not influence the surface hardness. Under cathodic protection, the metal surface only provides a location for the cathodic reaction, which is the reduction of O^2 to OH^-. And this process would not influence the surface mechanical properties in neutral and alkaline solutions. The contact depth is increased with the applied load, and the hardness is decreased slightly with the increase of the applied load.

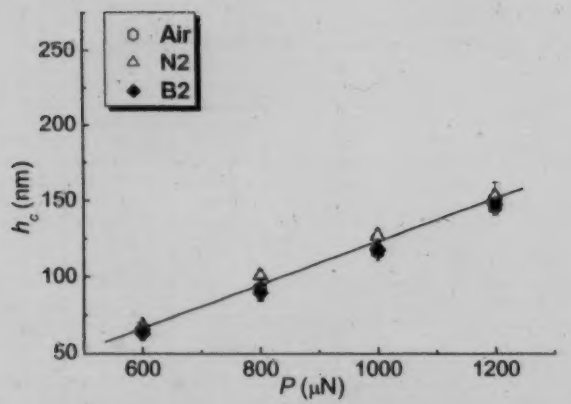

Figure 4-8 Contact depth with increasing of applied loads under CP

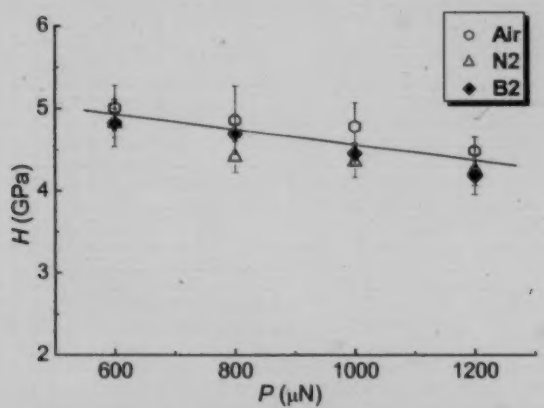

Figure 4-9 Surface hardness with increasing of applied loads under CP

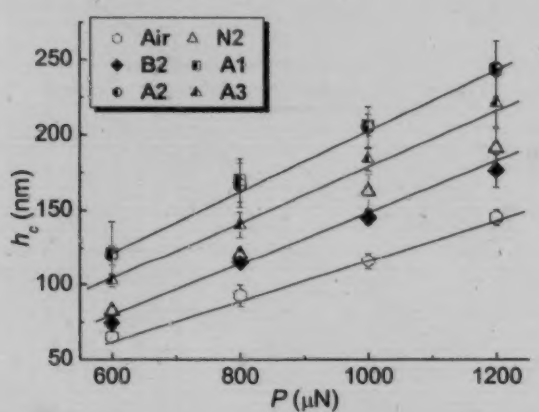

Figure 4-10 Contact depth with increasing applied loads under AD

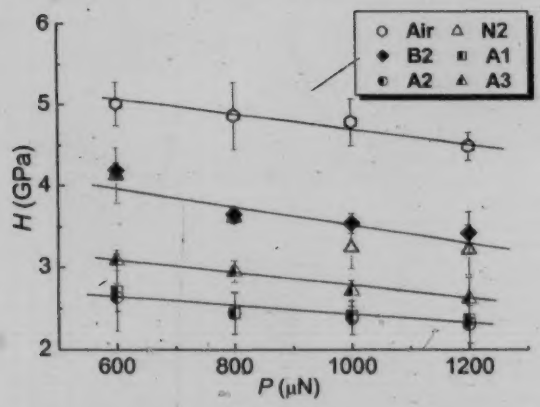

Figure 4-11 Surface hardness with increasing applied loads under AD

Under the anodic dissolution condition, in which the same current density was applied (1 mA/cm^2), the contact depth and surface hardness in all solutions are illustrated in **Fig. 4-10** and **Fig. 4-11** respectively. **Fig. 4-10** and **Fig. 4-11** show clearly that with an increasing applied load, the contact depth increases, while the hardness decreases. Under the anodic dissolution condition with the same applied load, the surface degradation (increased contact depth and decreased surface hardness) is more severe than that occurring under cathodic protection and in air. In neutral and alkaline solutions, the surface degradation is nearly the same, while in acid solutions, it is remarkably increased. In a series of acid solutions, it can be observed that the surface degradation is also dependent on the types of anions (SO_4^{2-} vs.Cl^-) under the galvanostatic control. **Fig. 4-12** shows the scanning surface morphologies by nanoindentation in different conditions: (a) in air; (b) under cathodic protection in 0.1 M Na_2SO_4; and (c) under anodic dissolution (i_{ap}=1 mA/cm^2) in 0.1 M Na_2SO_4. In all solutions, the

contact depth in anodic dissolution was deeper than that in a cathodic protection condition. It could be considered that the dissolving of iron atoms should be one reason explaining the difference of contact depth between anodic dissolution and cathodic protection conditions. Assuming the dissolving of iron atom is uniform and using Faraday's second law, the thickness of dissolved iron atoms can be calculated:

$$Thickness = \frac{i_{ap}}{zF}\frac{M_{Fe}}{\rho}t \qquad (4\text{-}1)$$

where $z = 2$, $F = 96{,}500$ C/mol, $M_{Fe} = 56$ g/mol, and the density of iron which = 7.8 g/cm^3, t (2 seconds) is the loading time. The thickness calculated using Faraday's law is about 0.75 nm, which is negligible compared to the difference of contact depth (10 nm at least) between those in air and those under anodic dissolution. This indicates that the dissolving of iron atoms has a very limited influence on the contact depth. The increased contact depth, hence hardness drop, during anodic dissolution is mainly caused by corrosion-induced localized surface plasticity [17,18].

The corrosion-induced localized surface plasticity is related to generation of vacancies caused by anodic dissolution [10,17,19,20]. The anodic overvoltage favors dissolution directly from ledge sites, even though the most energetically favorable dissolution atoms are from kink sites [10]. The vacancies might be injected into the sub-surface of metal by this non-uniform dissolution, hence

forming a supersaturation of vacancies [17,18,19]. Large amounts of vacancies attenuate the inter-atomic bonds of the metal surface, and result in the degradation of surface mechanical properties [21,22,23,24].

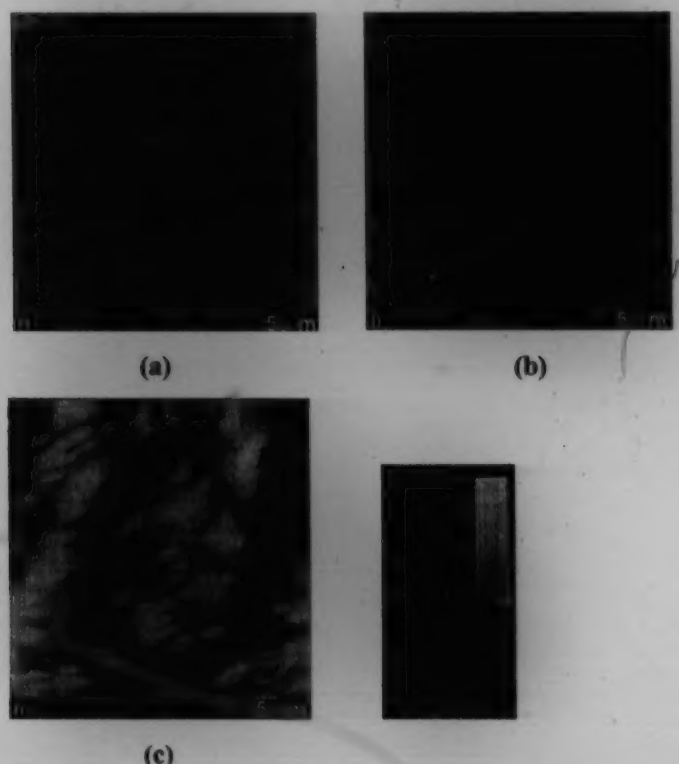

Figure 4-12 Surface morphologies in different conditions: (a) in air; (b) under cathodic protection in 0.1M Na_2SO_4; and (c) under anodic dissolution (i_{ap}=1 mA/cm^2) in 0.1M Na_2SO_4

In **Fig 4-10** and **Fig 4-11**, it can be observed that the degradation of mechanical properties in neutral and alkaline solutions was nearly same. However, in acid solutions, the degradation was much more serious compared those in neutral and alkaline solutions. There is another important issue which

should not be ignored: more serious degradation in acid solutions, compared to that in neutral and alkaline solutions. This applied current density is:

$$i_{ap} = i_a - |i_c| \Leftrightarrow i_a = |i_c| + i_{ap} \tag{4-2}$$

where i_{ap} is the applied current density, i_a is the actual anodic current density occurring on the iron surface, which is the actual dissolving rate of iron atoms, and i_c is the cathodic current density resulting from the cathodic reaction on the iron surface. **Eq. 4-2** indicates that the actual dissolving rate of iron does not only relate to the applied current density, but also to the cathodic current density. Although the applied current density is the same in **Fig. 4-10** and **Fig. 4-11**, i_a may not be the same if cathodic reaction current density i_c is not the same. To determine the value of i_a in the various solutions, the polarization curves in the active dissolution zone were measured. **Fig. 4-13** contains typical polarization curves to investigate i_a in different solutions (N2, B2, and A2) and they are all in the active dissolution zone. To calculate the cathodic current density, the extrapolation method was used in **Fig. 4-14**. The most linear part of the cathodic polarization zone was considered. This zone is indicative of the pure charge transfer occurring near OCP [25]. At a specific potential, the cathodic current density can be determined by extrapolating the linear segment of the cathodic reaction zone, as shown in **Fig. 4-14**. The horizontal line represents the polarized potential when i_{ap}=1 mA/cm^2, and the gradient line is the trended

linear line from the pure charge transfer zone. Thus, their intersection indicates the current density of the cathodic reaction rate. The results of i_a and i_c are listed in **Table 4-6**. They indicate that as in neutral and alkaline solutions, the polarization potential is not very similar to open circuit potential, and/or the self-current densities are smaller: the actual anodic current density is equal to the applied current density.

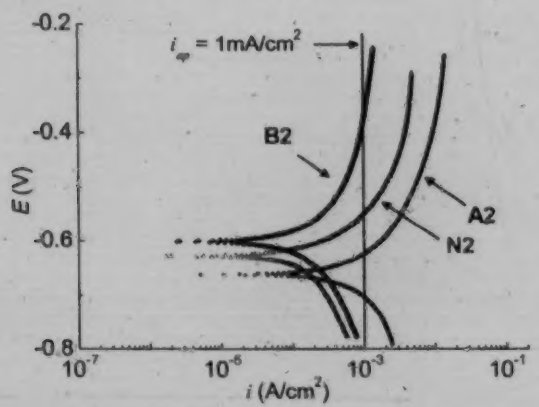

Figure 4-13 Polarization curves in different solutions

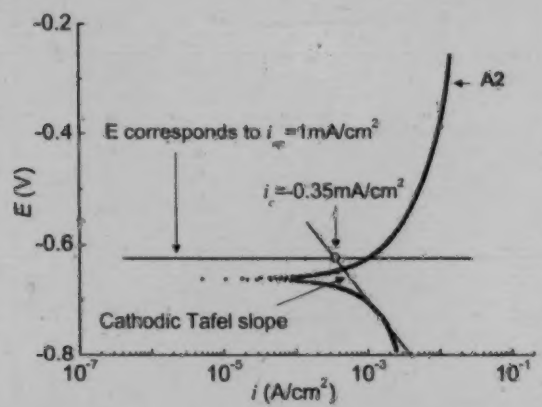

Figure 4-14 Extrapolation method to determine cathodic current density

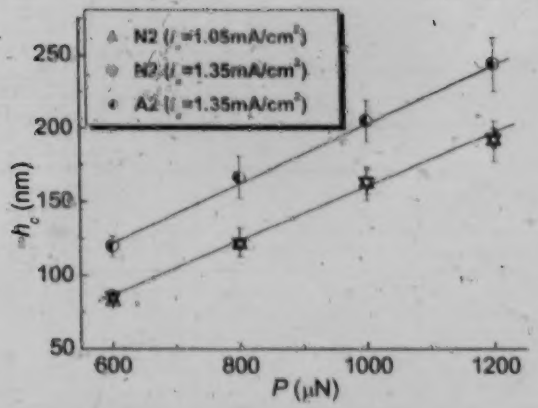

Figure 4-15 Contact depth measured under actual anodic dissolution

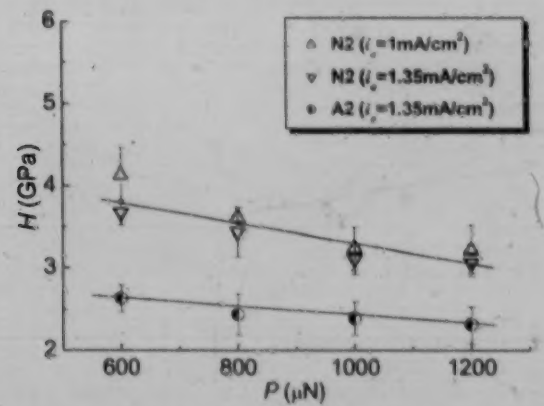

Figure 4-16 Surface hardness measured under actual anodic dissolution

Table 4-6 Actual cathodic and anodic current densities when i_{ap} was 1 mA/cm²

No.	Solution type	$\lvert i_c \rvert$ (mA/cm²)	i_a (mA/cm²)
N2	Neutral	0.05	1.05
B2	Alkaline	0.02	1.02
A2	Acid	0.35	1.35

The actual anodic current density represents the dissolution rate of iron atoms on the surface layer, hence influencing the vacancy generation rate. If the vacancy generation [10,17,18,19] is the only reason for the surface degradation, it is reasonable to predict that if the actual anodic dissolution rates are all the same in neutral, alkaline and acid solutions, the surface degradation should be the same as well. **Fig. 4-15** and **Fig. 4-16** show the contact depth and surface hardness respectively in neutral and acid solution with the actual anodic current density (i_a=1.35 mA/cm^2). It is clear that the contact depth and surface hardness dropped in neutral solutions with an increasing actual anodic current density, but they were not very similar to those in acid solutions, even with the same actual anodic current density. This phenomenon gives solid evidence that solution composition strongly influences the surface mechanical properties hence the erosion rate.

4.4 Discussions

4.4.1 Relationship between erosion-corrosion and surface mechanical properties

The relation of erosion-corrosion and corrosion-induced surface hardness drop was investigated using both theoretical and experimental measurements. It was indicated that the lower erosion rate with presence of corrosion is due to a corrosion-induced surface hardness drop [26,27].

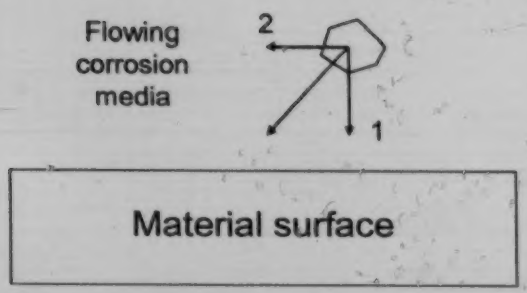

Figure 4-17 Schematic illustration of single sand impingement

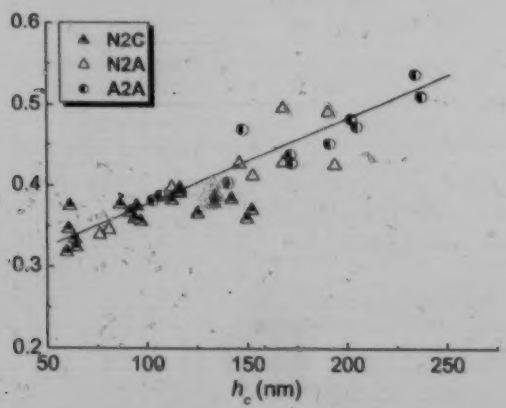

Figure 4-18 Friction coefficients with increasing of contact depth

The erosion process can be treated as the summation of every single impingement. In other words, the erosion rate in the same flowing condition is the summation of every single impingement in a given period of time. A possible simplified single impingement process at a specific angle is shown as **Fig. 4-17**. The process could be simply divided into two independent processes: (1) perpendicular hitting, or indent, and (2) cutting, or plowing. The indent process can be simulated by *in-situ* nanoindentation, and the plowing process can be investigated by *in-situ* nanoscratch. To correlate erosion-corrosion with surface

mechanical properties, we should know how processes (1) and (2) are influenced by the existence of corrosion, supposing that every single impingement has the same kinetic energy in all media as mentioned above.. This indicates that the vertical (1) and horizontal (2) kinetic energy is fixed in all corrosion media because the flowing parameters are kept the same. In the vertical condition, as the kinetic energy is fixed, it can be expected that the single impingement of sand would make a deeper contact depth on the surface with lower hardness, which is similarly shown in **Fig. 4-10** and **Fig. 4-11**. In the horizontal condition, along with a fixed horizontal kinetic energy, the parameter used to investigate the phenomenon is friction-coefficient by *in-situ* nanoscratch due to the fact that **Fig. 4-18**. **Fig 4-18** showed that the friction coefficient is a linear function of contact depth. Deeper indentation would induce a higher friction coefficient, resulting in lower speed of sand when leaving the material surface after impinging, hence more plowing energy passing to the material surface and causing more severe plowing. Thus, higher material volume loss or material mass loss is caused by this effect. In this case, the correlation has been established between nano indent and erosion material loss. Lower hardness causes deeper indent/contact depth, and more severe plowing, resulting in higher material loss.

4.4.2 Effect of solution compositions on erosion resistance and surface mechanical properties

The hardness and contact depth give a good explanation of higher erosion with the presence of corrosion current. However, anodic current is not the only parameter that influences the erosion rate; it is also influenced by solution composition in the presence of corrosion current. In present work, the solution composition that influences the erosion rate is mainly divided into two groups: acid and neutral/alkaline. From the erosion-corrosion and *in-situ* nanoindentation tests, it could be summarized that in neutral and alkaline solutions, under the same flowing condition, the erosion rate is almost independent of solution composition, and it is only related to anodic current density, while in acid solutions, the solution composition makes a bigger contribution than applied current. By changing the H^+ concentration and replacing it by Na^+ under the same galvanostatic control shown in **Fig. 4-7** (SO_4^{2-}: group A vs. group B, and Cl^-: group C vs. group D), one could draw the conclusion that the H^+ concentration does not affect the erosion rate, while anions (SO_4^{2-} vs. Cl^-) do. Without the presence of H^+, the erosion rate is not influenced by types of anions. Both erosion-corrosion weight loss and *in-situ* nanoindentation tests indicate that with presence of H^+, different anions will give different degradation on surface mechanical properties hence different erosion rates, while the concentration the of solution is not a major control parameter.

As anodic dissolution injects vacancies into the surface of material, and the vacancies generation rate should be related to dissolution rate of materials, there is still no explanation as to why in acid solutions there is more severe degradation. How anions influence the mechanical properties and erosion resistance in acid solutions is also unknown. Further work should be done to clearly understand these phenomena.

4.5 Conclusions

1. The solution composition influences erosion-corrosion when there are hydrogen ions in the solution. In other words, in an acid solution, the solution composition greatly influences the erosion-corrosion behavior, but in neutral or base solutions, it does not.
2. In acid solutions under the same galvanostatic control, the erosion rate and the surface degradation depend on the types of anions rather than the H^+ concentration.
3. *In-situ* nanoindentation confirms that surface degradation with the presence of corrosion in present work is at least one of mechanisms of corrosion-induced erosion.

References

[1] M.M. Stack, B.D. Jana, "Modelling particulate erosion-corrosion in aqueous slurries: Some views on the construction of erosion-corrosion

maps for a range of pure metals", Wear, v256 (2004), pp. 986-1004.

[2] M.M. Stack, N. Pungwiwat, "Particulate erosion-corrosion of Al in aqueous conditions: Some perspectives on pH effects on the erosion-corrosion map", Tribology International 35, n 10, p.651-660.

[3] Y. Li, G.T. Burstein, I.M. Hutchings, "Influence of environmental composition and electrochemical potential on the slurry erosion-corrosion of aluminium", Wear 181-183, n 1 (1995), p.70-79.

[4] Y.X. Zhou, Z.L. Lu, M. Zhan, "An investigation of the erosion–corrosion characteristics of ductile cast iron", Materials and Design 28 (2007), pp. 260-265.

[5] B.D. Jana; M.M. Stack, "Modeling impact angle effects on erosion-corrosion of pure metals: Construction of materials performance maps" Wear 259, n 1-6 (2005), p.243-255.

[6] Q. Ma, D.R. Clarke, "Size Dependence of the Hardness of Silver Single Crystals" Journal of Materials Research 10 (1995), pp. 853-863.

[7] K.W. McElhaney, J.J. Wlassak, W.D. Nix, "Determination of Indenter Tip Geometry and Indentation Contact Area for Depth-sensing Indentation Experiments", Journal of Materials Research 13 (5) (1998), pp. 1300-1306.

[8] N.A Fleck, J.W. Hutchinson, "Phenomenological theory for strain gradient effects in plasticity", Journal of the Mechanics and Physics of Solids 41 (1993), pp. 1825-1857.

[9] N.A. Fleck, G.A. Muller, M.F. Ashby, J.W. Hutchinson, "Strain gradient plasticity: theory and experiment", Acta Metallurgica and Materialia 42 (1994), pp. 475-487.

[10] W. D. Nix, H. Gao, "Indentation size effects in crystalline materials: a law for strain gradient plasticity", Journal of Mechanics and Physics Solids, (1998) 46 (3), pp. 411-425.

[11] S. Yin, D.Y. Li, "Effects of prior cold work on corrosion and corrosive wear of copper in HNO_3 and NaCl solutions", Materials Science and Engineering A 394 (2005), p. 266.

[12] C. Montero-Ocampo, L. Veleva, "Corrosion of Carbon Steel in Aerated 3% Sodium Chloride", Corrosion 58 (2002), p. 601-607.

[13] J.H. Xie, A.T. Alpas, D.O. Northwood, "Mechano-electrochemical effect between erosion and corrosion", Journal of Materials Science 38 (2003), pp. 4849-4856.

[14] H.X. Guo, B.T. Lu, J.L. Luo, "Interaction of mechanical and electrochemical factors in erosion-corrosion of carbon steel", Electrochimica Acta 51 (2005), p. 315-323.

[15] B. Gu, W.Y. Chu, W. Chu, L.J. Qiao, C.M. Hsiao, "Effect of anodic polarization on the ambient creep of brass", Corrosion Science 36 (8) (1994), pp.1437-1445

[16] H.X. Guo, B.T. Lu, J.L. Luo, "Response of surface mechanical properties to electrochemical dissolution determined by in situ nanoindentation technique", Electrochemistry Communications, v8, pp. 1092-1098.

[17] D.A. Jones, "A united mechanism of stress corrosion and corrosion fatigue cracking", Metallurgical Transactions A 16 (1985), pp.1133-1141.

[18] D.A. Jones, "Localized surface plasticity during stress corrosion cracking", Corrosion 52 (5) (1996), pp. 356-362.

[19] D.A. Jones, A.F. Jankowski, "Anodically enhanced. diffusion in Cu/Ag

thin film couples", Scripta Metallugica and Materialia, 29 (1993), p.701.

[20] D.A. Jones, A.F. Jankowski, G.A. Davidson, "Room-temperature diffusion in Cu/Ag thin-film couples caused by anodic dissolution", Metallurgical and Materials Transactions A 28 (1997), p. 843.

[21] C.H. Caceres, B.I. Selling, "Casting defects and the tensile properties of an Al-Si-Mg alloy", Materials Science and Engineering A 220 (1996), pp. 109-116.

[22] N. Chawla, X. Deng, "Microstructure and mechanical behavior of porous sintered steels", Materials Science and Engineering A 390 (2005), p. 98.

[23] A. Hadrboletz, B. Weiss, "Fatigue behaviour of iron based sintered material: A review", International Materials Reviews 42 (1997), pp.1-44.

[24] C. Tekmen, I. Ozdemir, U. Cocen, K. Onel, "The mechanical response of Al-Si-Mg/SiC_p composite: Influence of porosity", Materials Science and Engineering A 360 (2003), pp. 365-371.

[25] G. Kear, F.C. Walsh, "The characteristics of a true Tafel Slope", Corrosion and Materials 30 (6) (2005), p.S-1.

[26] B, T. Lu and J. L. Luo, "Prediction of Synergistic Effect in Erosion Corrosion", submitted to Corrosion Science (2007).

[27] E.M. Gutman, Mechanochemistry of Materials, Cambridge International Science Publishing, Great Abington, Cambridge, UK (1998)

Chapter 5

Correlation between Repassivation Kinetics and Corrosion Rate over a Passive Surface in Flowing Slurry

5.1 Introduction

As demonstrated by many researchers, the accelerated corrosion in fluids is mainly attributed to the promoted mass transfer in the boundary layer of the liquid at the electrolyte interface [1,2,3,4,5]. However, corrosion reactions are not always controlled by mass transfer processes [4,5]. If the target material is in a passive state, the slurry impingement may cause damage or breakdown of its passive films, hence remarkably increasing the corrosion process [6,7,8,9,10]. Some investigations show that the breakdown of passive film due to particle impingement is the main mechanism for erosion-enhanced corrosion of passivated metals in flowing slurries [1,2,4]. This indicates that the erosion-enhanced corrosion of a passive electrode depends not only on the hydrodynamic parameters and the corrosivity of the flowing slurries, but also on the mechanical properties and the electrochemical characteristics of the passive film [1,2,11,12]. Although corrosion often contributes only a small portion of the total material loss in flowing slurries, it promotes mechanical erosion

markedly, as indicated by the fact that the erosion rate increases with the corrosion current density [13,14]. Ferrer et al. [15] and Neville et al. [16] measured the electrochemical response of stainless steels impacted by a single glass bead. However, the explanations provided for the erosion-enhanced corrosion of passive metals are still qualitative [1,2,10,11,15,16]. The objective of this chapter is to find a quantitative way to correlate corrosion current density to current response caused by the impingement of single particles.

The present model to correlate corrosion current density and repassivation kinetics was developed by Lu *et al.* [17]. My contributions are to provide all of the experimental data related to carbon steel to support the model's prediction.

5.2 Experimental details

Table 5-1 Experimental conditions

Sample	Sand concentration (%wt.)	E (VSCE)
AISI 1018	10, 15, 20, 25, 30, 35, 40	0, 0.2, 0.6
AISI 1045	5, 10, 15, 20, 25, 30, 35	0.2, 0.8

Table 5-2 Test solutions

Solutions	Composition
0.1 M Borate buffer	0.1M H_3BO_3 + 0.025M $Na_2B_4O_7$
0.3 M Borate buffer	0.3M H_3BO_3 + 0.075M $Na_2B_4O_7$

In order to investigate the correlation of current density to current response, the rotating electrode cylinder system and the scratch system were used. Descriptions of these two systems can be found in **Chapter 3**. The rotating electrode cylinder system was used to test the erosion-corrosion rate in flowing slurries under different applied potentials. Two kinds of low carbon steel, AISI1018 and AISI1045, were used in this test. The experimental conditions are listed in **Table 5-1**. The electrolytes used are the borate buffer solutions listed in **Table 5-2**. The experimental conditions for the rotating electrode cylinder system and the scratch system were the same.

5.3 Results

5.3.1 Corrosion current density in rotating slurry

The polarization curves of A1018 and A1045 steels are illustrated in **Fig. 5-1**. They indicate that the test materials were passivated in the flowing slurries prepared using the borate buffer solutions under the test conditions. The polarization potentials start from about -0.4 V_{SCE} in all conditions. The potentials chosen for the rotating tests are all in the passive range. Also, reversed potential scans were carried out. The reversed polarization curves nearly overlap the original polarization curves. This indicates that the pitting probably does not occur, because the impingement of sand breaks down the enclosed environment and stops the propagation of the pitting.

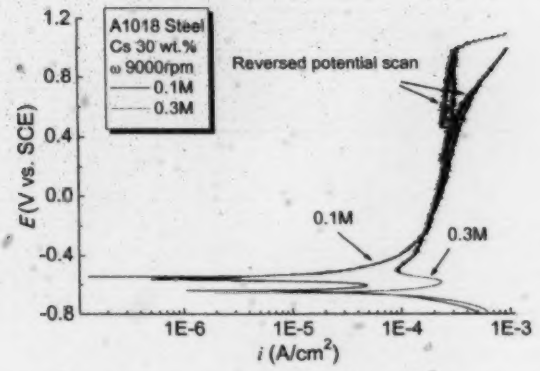

(a)

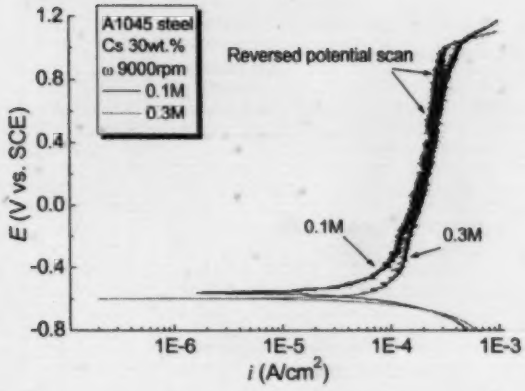

(b)

Figure 5-1 Polarization curves of (a) A1018 and (b) A1045 in slurries with different solution concentrations

("Cs" is the sand concentration, and "ω" is the rotating speed)

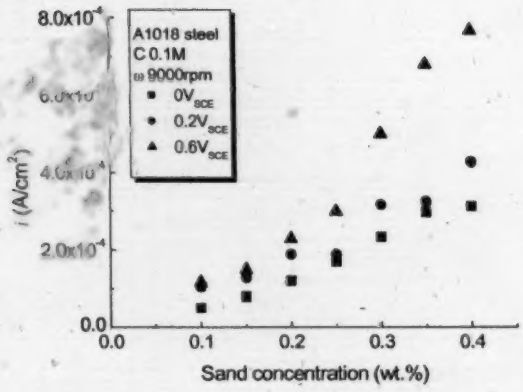
A1018 steel
C 0.1M
ω 9000rpm
0V SCE
0.2V SCE
0.6V SCE
i (A/cm²)
Sand concentration (wt.%)

(a)

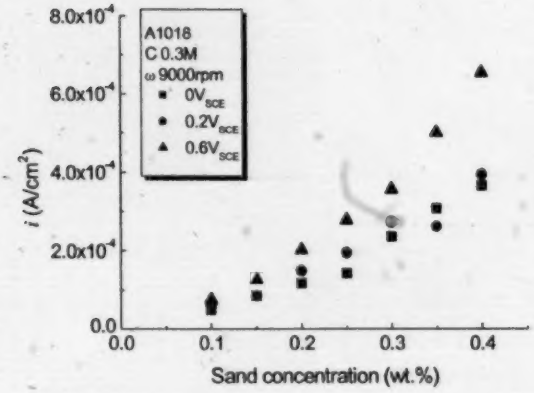
A1018
C 0.3M
ω 9000rpm
0V SCE
0.2V SCE
0.6V SCE
i (A/cm²)
Sand concentration (wt.%)

(b)

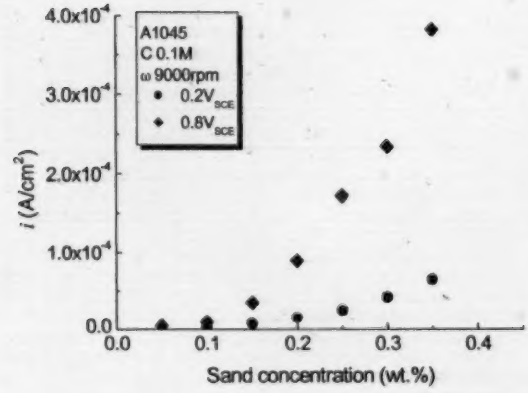
A1045
C 0.1M
ω 9000rpm
0.2V SCE
0.8V SCE
i (A/cm²)
Sand concentration (wt.%)

(c)

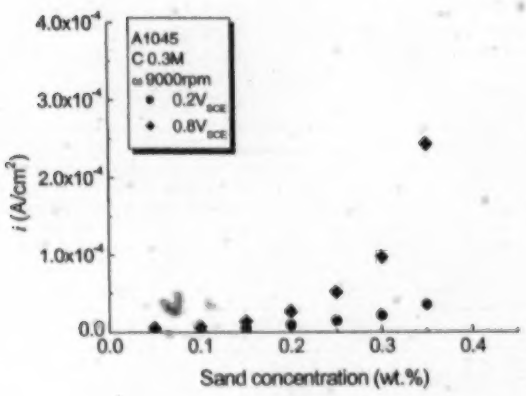

(d)

Figure 5-2 Erosion-corrosion current densities of (a) and (b) A1018 and (c) and (d) A1045 in slurries with the solution concentrations of (a) and (c) 0.1 M, and (b) and (d) 0.3 M. ("C" is the solution concentration)

Fig. 5-2 shows the current densities of steels while they were rotated in the slurries. It clearly illustrates that the current densities increase as the sand concentration increases. The explanation for this is that higher sand concentrations result in more sand impingements in a given time, hence breaking down more of the passive film. Therefore, it causes larger fresh metal areas to be exposed to the solution, resulting in a higher corrosion current density. In **Fig. 5-2**, another phenomenon is shown. When the potential, sand concentration and the type of steel are fixed, the corrosion current density is higher in more condensed solutions than it is in more diluted solutions. The reason might be that when the passive film on the surface is broken down by the impingement of sand, the more condensed solution has a higher conductivity and mass transfer; hence the corrosion current density is higher.

5.3.2 Current decay in scratch test

Slurry impingement may cause damage or breakdown of passive films and thereby significantly accelerate the corrosion process [1,2,4]. The scratch test can be used to simulate the current response to impingement by sand particles. **Fig. 5-3** clearly shows the typical current decay curves of A1018 and A1045 steels in the borate buffer solution.

In the scratch process, there is a sharp current rise. After trending these decay curves, it shows that the repassivation kinetics can be formulated approximately as:

$$i = i_S + \alpha t^{-\beta} = i_S + i_{Peak}\left(\frac{t}{\tau_0}\right)^{-\beta} \qquad t > \tau_0, 0 < \beta < 1 \qquad (5\text{-}1)$$

where α and β are experimental constants; $0 < \beta < 1, \alpha = i_{peak}\tau_0^{\beta}$, i_s is the stable passive current density under erosion-free conditions, i_{peak} is the peak response of local current density to the impingement. The average values of α, β, i_{peak}, and τ_0 for the test materials are given in **Table 5-3**. It is still difficult to formulate the current density of the carbon steels after scratched in a borate buffer solution when $t < \tau_0$. To simplify the analysis, the current density over the scratched surface is considered to be the peak current density,

$$i = i_S + i_{peak} \qquad t \le \tau_0 \qquad (5\text{-}2)$$

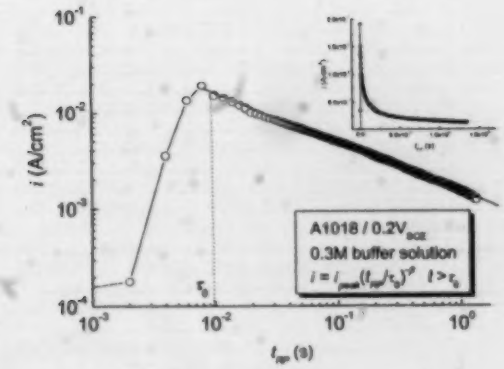

(a)

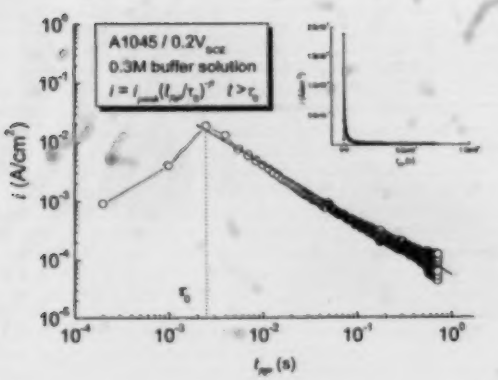

(b)

Figure 5-3 Power law of the current decay of A1018 and A1045 steels

Table 5-3 Parameters of repassivation kinetics for carbon steels (τ_0=0.01s)

Steel	Buffer Solution	E (V_{SCE})	β	i_s ($10^{-6}A/cm^2$)	i_{peak} ($10^{-2}A/cm^2$)
A1018	0.1 M	0	0.74±0.03	3.5±0.5	2.45±0.82
		0.2	0.79±0.07	3.9±0.6	4.14±0.83
		0.6	0.83±0.11	4.3±0.3	7.47±0.67
	0.3 M	0	0.76±0.12	3.9±0.5	1.92±0.72
		0.2	0.74±0.12	4.2±0.6	2.07±0.94
		0.6	0.77±0.07	4.5±0.3	2.09±0.69
A1045	0.1 M	0.2	0.75±0.11	4.0±0.5	5.67±1.56
		0.8	0.76±0.10	4.5±0.9	3.89±1.16
	0.3 M	0.2	0.79±0.11	4.3±0.3	1.26±0.35
		0.8	0.80±0.12	4.4±0.6	0.96±0.38

Table 5-4 Sand particle properties

ρ_p (kg/m^3)	$\overline{V}_p$ (m^3)	$\overline{d}_p$ (mm)
2560	$1.21\times10^{-11}\pm1.2\times10^{-12}$	$2.85\times10^{-4}\pm2.8\times10^{-5}$

5.3.3 Correlation between corrosion current density and repassivation kinetics

Before correlating the relationship between corrosion current density and repassivation kinetics, some assumptions are necessary. Lu *et al.* [17,18]

established a theoretical model to correlate the corrosion rate of passive metals to the repassivation kinetics under stable conditions, based on the following assumptions.

1. The target material and the passive film on its surface have uniform electrochemical and mechanical properties.
2. The mass, size, and shape of all impinging particles are identical and they are non-deformable.
3. The surface roughness and the strain hardening in the surface layer do not change before or after the tests.
4. The momentum of individual particles is assumed to be the same. A uniform flux of solid particles J_p over the target surface can be expressed as

$$J_p = C_p U \sin\theta \tag{5-3}$$

where C_p is the weight of solid particles in the slurry with the unit volume; U is the impact velocity; and θ is the impact angle. As a consequence, the normalized fresh surface generating rate caused by the particle impingement $\dot{A}_e$ is formulated by (more details are in **Reference 17** and **18**)

$$\dot{A}_e = n_i \overline{A}_{crater} = \left(\frac{J_p}{\overline{m}_p}\right)\overline{A}_{crater} = \left(\frac{C_p U \sin\theta}{\rho_p \overline{V}_p}\right)\overline{A}_{crater} \tag{5-4}$$

where ρ_p, $\overline{m}_p$, and $\overline{V}_p$ are the density, the average mass, and the volume of sand particle respectively, n_i is the impingement frequency over an electrode surface with unit area, and $\overline{A}_{crater}$ is the average crater caused by every single particle impingement.

5. The particle impingement is the sole mechanism resulting in erosion and passive film breakdown. As a result of assumptions 1 through 4, each particle impingement removes the same amount of material from the surface and produces a crater of the same volume, surface area, and shape, leading to an identical electrochemical response.

6. The response of local current density to individual particle impingement includes a rapid rise in the local current density over the impacted area due to the passive film breakdown and a relatively slow recovery through repassiviation, where i_{peak} is the peak response of local current density to the particle impingement and i_s is the stable passive current under the erosion-free conditions.

7. Multiple impingements do not change the peak response of local current density to the impingement i_{peak} or the repassivation kinetics after impingement. This means that, when the test condition is held unchanged, the local current density i, at a given point on the target surface, peaks immediately after impact by the solid particle and its value is always equal to $i_S + i_{peak}$, no matter what value the local current density is on the crater surface before the impingement. After the impingement, the local current

density over the crater surface decays always following same pattern, and the kinetic parameters of repassivation are not affected by the repeated particle impingements. This means that, as a first approximation, an identical correlation is assumed to be held between the local current density at the location impacted by a solid particle and the time elapsed after the particle impingement at this location.

According to assumption 6, the corrosion current density over a surface will be non-uniformly distributed when impacted by slurry. In line with the kinetic analysis of slurry impingement, the average current density over the whole electrode surface $\bar{i}$ can be expressed as [18,17]

$$\bar{i} = \frac{1}{A}\int_0^A i\, dA = \int_0^1 i\, d\Lambda = \dot{A}_e \int_0^\infty i \exp\left(-\dot{A}_e t\right) dt \qquad (5\text{-}5)$$

where A is the surface area of the electrode, the non-dimensional parameter $d\Lambda = dA/A$ represents the area fraction of the electrode surface on which the local current density is equal. Based on assumptions 4, 6, and 7, the local current density $i = i(t)$ under a given test condition is a function of the time elapsed after the last particle impingement at this location and depends on the kinetic model of repassivation.

When we insert **Eq. 5-1** and **Eq. 5-2** into **Eq. 5-5**, we get:

$$\bar{I} = \dot{A}_e \int_0^{\infty} i \exp\left(-\dot{A}_e t\right) dt = \dot{A}_e \int_0^{\tau_0} i \exp\left(-\dot{A}_e t\right) dt + \dot{A}_e \int_{\tau_0}^{\infty} i \exp\left(-\dot{A}_e t\right) dt$$

$$= i_S + i_{peak} \int_0^{\tau_0} \exp(-\dot{A}_e t) d(\dot{A}_e t) + i_{peak} \dot{A}_e \tau_0^{\beta} \int_0^{\infty} t^{-\beta} \exp(-\dot{A}_e t)\, dt$$

$$- i_{peak} \dot{A}_e \tau_0^{\beta} \int_0^{\tau_0} t^{-\beta} \exp(-\dot{A}_e t) dt \qquad (5\text{-}6)$$

Define $\lambda = \tau \dot{A}_e$ and $u = \dot{A}_e t$, **Eq. 5-6** becomes

$$\bar{I} = i_S + i_{peak} \int_0^{\lambda_0} e^{-u} du + i_{peak} \lambda_0^{\beta} \int_0^{\infty} u^{-\beta} e^{-u}\, du - i_{peak} \lambda_0^{\beta} \int_0^{\lambda_0} u^{-\beta} e^{-u} du \qquad (5\text{-}7)$$

Then define

$$\Gamma(1-\beta) = \int_0^{\infty} u^{-\beta} e^{-u} du \qquad 0 < \beta < 1 \qquad (5\text{-}8)$$

We then have

$$\bar{I} = i_S + i_{peak} (1 - e^{-\lambda_0}) + i_{peak} \lambda_0^{\beta} \Gamma(1-\beta) - i_{peak} \lambda_0^{\beta} \int_0^{\lambda_0} u^{-\beta} e^{-u} du \qquad (5\text{-}9)$$

In most cases of the present study, $\tau_0 = 0.01\,\text{s}$, $U \le 10\,\text{m/s}$, $C_p \le 500\,\text{kg/m}^3$, the sand particle diameter is less than 0.5mm, the density of sand particle is about 2.6, and $\bar{A}_{crater} \le 1\times10^{-10}\,\text{m}^2$. When using the data to calculate λ_0, $\lambda_0 < 0.07 << 1$. Therefore, $e^{-\lambda_0} \approx 1 - \lambda_0$. In the range $0 < \beta < 1$, $\Gamma(1-\beta) \approx 1/(1-\beta)$, as shown in **Fig. 5-4**. Thus, **Eq. 5-9** can be simplified by

taking the first order approximation:

$$\bar{i} \approx i_s + i_{peak}\frac{1}{1-\beta}\lambda_0{}^{\beta} - i_{peak}\frac{\beta}{1-\beta}\lambda_0 = i_S + \frac{i_{peak}}{1-\beta}\left(\lambda_0^{\beta} - \beta\lambda_0\right) \tag{5-10}$$

Eq. 5-10 is the function by which the correlation of the repassivation kinetics and corrosion current density is made in present work.

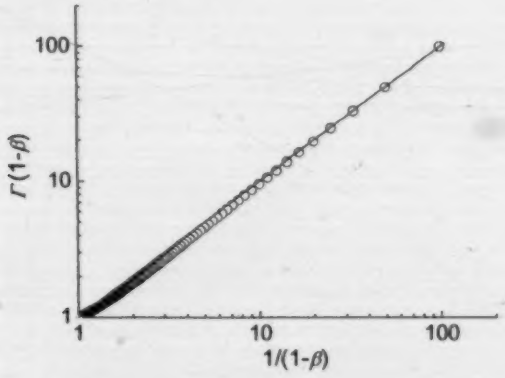

Figure 5-4 Gamma function

5.3.4 Calculation details and predicted results

In order to make a prediction using **Eq. 5-10**, some more data are needed. As i_S, i_{peak}, and β are known from the scratch tests, listed in **Table 5-3**, the only other thing necessary for this prediction is λ_0. As it is known that $\lambda = \tau \bar{A}_e$, by inserting **Eq. 5-4** into **Eq. 5-10**, we get

$$\lambda_0 = \tau_0 n_i \bar{A}_{crater} = \tau_0 \left(\frac{C_p U \sin\theta}{\rho_p \bar{V}_p}\right)\bar{A}_{crater} \tag{5-11}$$

Because the density of sand is larger than that of the water, the sand concentration of slurry in an RCE system is non-uniformly owing to action of the centrifugal force. The direct measurement of the average sand concentration over the specimen surface is difficult. In the present study, an attempt is made to correlate the corrosion current density to the erosion wastage. If the particle impingement is the sole source of erosion, the total material loss rate caused by the erosion e can be correlated to the average volume of a material removed by a single impingement $\overline{V}_{crater}$ as follows

$$e = n_i \rho \overline{V}_{crater} \tag{5-12}$$

where ρ is the density of the target material. As a consequence, the ratio of the fresh surface generating rate caused by particle impingement and the erosion wastage can be related to the ratio of the surface area to the volume for a crater y in the following form [18,17]:

$$y = \frac{\overline{A}_{crater}}{\overline{V}_{crater}} = \rho \frac{\dot{A}_e}{e} \tag{5-13}$$

Insert **Eq. 5-13** into **Eq. 5-11**, we get:

$$\lambda_0 = \frac{\tau_0 y e}{\rho} \tag{5-14}$$

In the RCE system, the impingement angle is small and hence the erosion is dominated by the cutting mechanism, as demonstrated by the SEM observation in **Fig. 5-5**. In this case, the ratio of surface area to volume for a crater produced by the cutting can be approximately formulated by [18,17]

$$y = \mu \frac{\bar{d}_p}{\bar{w}_{crater}^2} \tag{5-15}$$

where $\bar{w}_{crater}$ is the average width of cater, $\bar{d}_p$ is the mean diameter of particle, μ is a constant approximately equal to 1.75. Therefore from **Eq. 5-15** and **Eq. 5-14**, we get:

$$\lambda_0 = \frac{\mu \bar{d}_p \tau_0 e}{\rho \bar{w}_{crater}^2} \tag{5-16}$$

Insert **Eq. 5-16** into **Eq. 5-10**, and we get

$$\bar{i} = i_s + \frac{i_{peak}}{1-\beta}\left[\left(\frac{\tau_0 \mu \bar{d}_p e}{\rho \bar{w}_{crater}^2}\right)^{\beta} - \beta \frac{\tau_0 \mu \bar{d}_p e}{\rho \bar{w}_{crater}^2}\right] \tag{5-17}$$

Figure 5-5 Craters created by sand impingements in 1%wt sand slurry

Eq. 5-17 can be used to correlate the corrosion current density to the erosion rate. The parameters on the right side of the equation can be determined experimentally. The density of carbon steel is 7.8 g/cm^3. The values of $\overline{w}_{crater}$ can be measured from SEM images of craters, as shown in **Fig. 5-5**, and are between 81 μm to 146 μm, depending on the test conditions. The values of the other parameters are listed in **Table 5-3** and **Table 5-4**.

In **Eq. 5-17**, $\overline{w}_{crater}$ is the width of the crater with the existence of a corrosion current. Due to rapid anodic dissolution, the crater sizes were difficult to measure accurately when erosion-corrosion tests were conducted. This phenomenon was obvious especially when the specimens were polarized at a high voltage, i.e. 0.6 V_{SCE} or 0.8 V_{SCE}. Because of this, the $\overline{w}_{crater}$ was determined using the following method [17]:

1. Measure the erosion rates under the cathodic protection and the anodic polarization conditions, respectively.

2. Measure the average crater sizes under the cathodic protection condition using SEM
3. Assume that the anodic dissolution does not change the crater's geometric shape and that the ratio of average crater volumes under the anodic polarization and cathodic protection conditions is equal to the ratio of erosion rates under these two conditions, the average crater width under the anodic polarization condition $\overline{w}_{crater,AP}$ will be given by

$$\overline{w}_{crater,AP} = \left(\frac{e}{e_0}\right)^{1/3} \overline{w}_{crater,CP} \tag{5-18}$$

where e_0 is the erosion rate under the cathodic protection condition, $\overline{w}_{crater,CP}$, and e are the average crater width and erosion rate under the cathodic protection condition, respectively.

The second term in the bracket on the right side of **Eq. 5-17** represents the contribution of current before current decay occurs ($t_{RP} < \tau_0$). When $\lambda_0 << 1$, $\beta\lambda_0 >> \lambda_0^{\beta}$ because $\beta << 1$. **Eq. 5-17** can be simplified into

$$\bar{i} \approx i_S + \frac{i_{peak}}{1-\beta}\left(\frac{\tau_0 \mu \overline{d}_p e}{\rho \overline{w}_{crater}^2}\right)^{\beta} \tag{5-19}$$

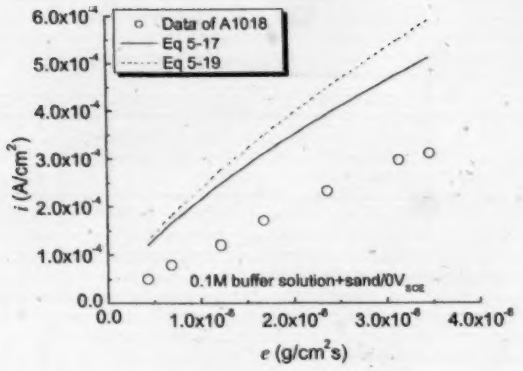
Data of A1018
Eq 5-17
Eq 5-19
0.1M buffer solution+sand/0V$_{SCE}$
i (A/cm^2)
e (g/cm^{2}s)

(a)

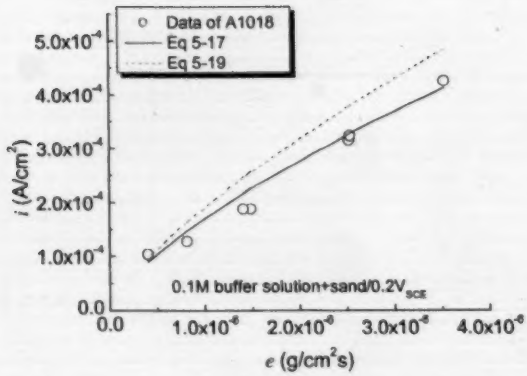
Data of A1018
Eq 5-17
Eq 5-19
0.1M buffer solution+sand/0.2V$_{SCE}$
i (A/cm^2)
e (g/cm^{2}s)

(b)

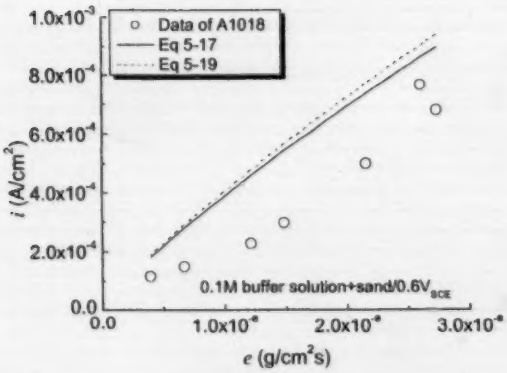
Data of A1018
Eq 5-17
Eq 5-19
0.1M buffer solution+sand/0.6V$_{SCE}$
i (A/cm^2)
e (g/cm^{2}s)

(c)

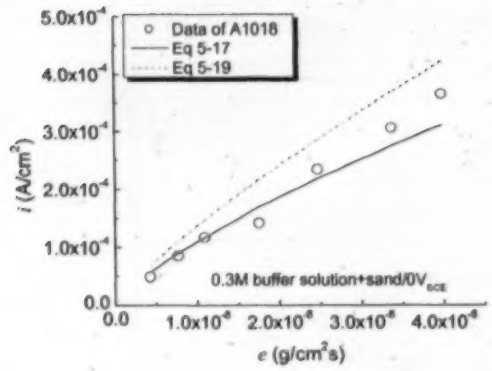

(d)

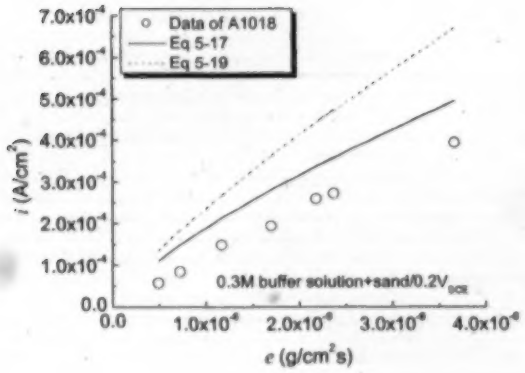

(e)

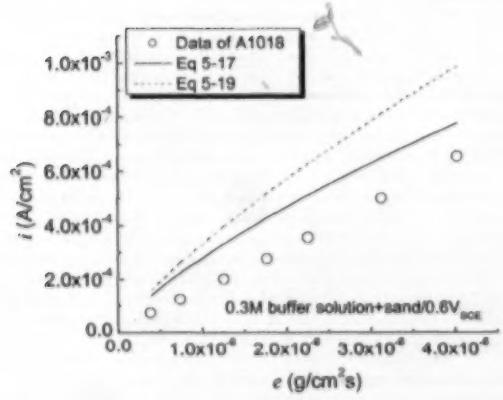

(f)

Figure 5-6 Correlation between current densities of A1018 and erosion rates

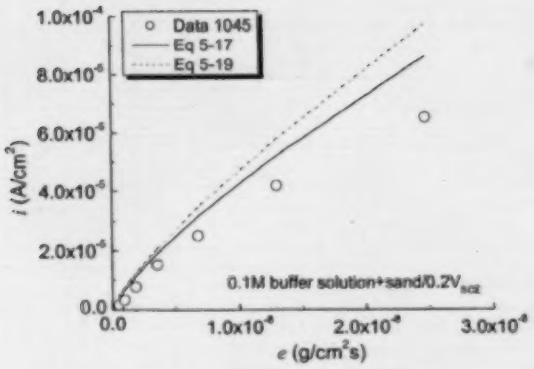
Data 1045
Eq 5-17
Eq 5-19
0.1M buffer solution+sand/0.2V$_{SCE}$
i (A/cm^2)
e (g/cm^{2}s)
1.0x10^{-4}
8.0x10^{-5}
6.0x10^{-5}
4.0x10^{-5}
2.0x10^{-5}
0.0
1.0x10^{-6}
2.0x10^{-6}
3.0x10^{-6}

(a)

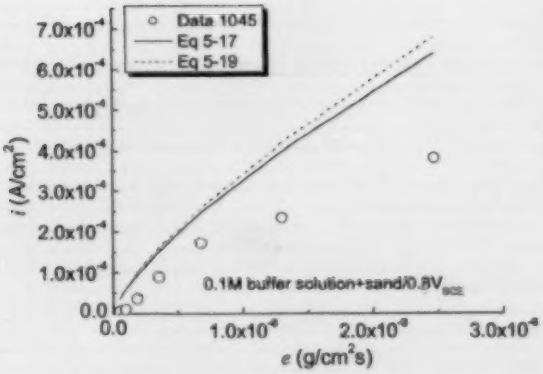
Data 1045
Eq 5-17
Eq 5-19
0.1M buffer solution+sand/0.8V$_{SCE}$
i (A/cm^2)
e (g/cm^{2}s)
7.0x10^{-4}
6.0x10^{-4}
5.0x10^{-4}
4.0x10^{-4}
3.0x10^{-4}
2.0x10^{-4}
1.0x10^{-4}
0.0
1.0x10^{-6}
2.0x10^{-6}
3.0x10^{-6}

(b)

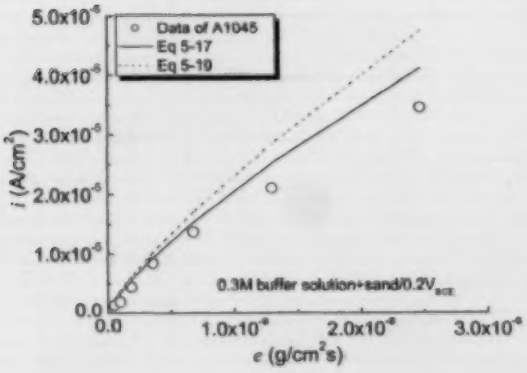
Data of A1045
Eq 5-17
Eq 5-19
0.3M buffer solution+sand/0.2V$_{SCE}$
i (A/cm^2)
e (g/cm^{2}s)
5.0x10^{-5}
4.0x10^{-5}
3.0x10^{-5}
2.0x10^{-5}
1.0x10^{-5}
0.0
1.0x10^{-6}
2.0x10^{-6}
3.0x10^{-6}

(c)

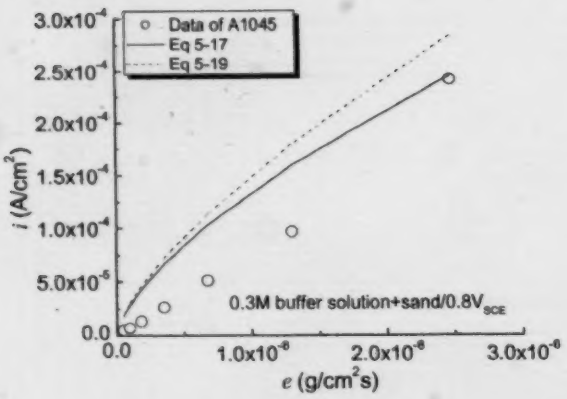

(d)

Figure 5-7 Correlation between current densities of A1018 and erosion rates

The results in **Fig. 5-6** and **Fig. 5-7** indicate that **Eq. 5-19** can still provide reasonable predictions to the corrosion current density of carbon steels under the present test conditions.

5.4 Discussions

5.4.1 Measurements of repassivation kinetics

The effect of fluid dynamic parameters on corrosion rate in flowing media depends on the corrosion mechanism. When the corrosion rate is completely controlled by the mass transfer of dissolved oxygen in the boundary layer at the electrode/electrolyte interface, the corrosion rate is proportional to the limited current density of dissolved oxygen and is independent of the properties of the target material [1,4,5,19]. If corrosion is controlled by the electric charge

transfer process under the active dissolution condition, the corrosion will be promoted by the dynamic plastic deformation produced by the impingement of solid particles [20]. In this case, the mechanical properties of the target material will affect the corrosion rate.

For the passive system, if the passive film is damaged by particle impingement in the slurry, the anodic dissolution rate over the damaged surface is governed by the repassivation. The repassivation depends on the electrochemical characteristics of the target material, electrolyte, temperature and fluid dynamics of the media [7,18]. Some researchers have pointed out that an increase in flowing velocity [1] could influence the mass transport process at the electrode/electrolyte interface and that the impingement angle can affect the local current response [21]. In present work, as scratch tests were performed in stagnant solutions and the movement of the scratch tip was always parallel to the target surface, the hydrodynamic effects of corrosive media on repassivation could not be well simulated.

5.4.2 Galvanic effect

Theoretically, in the present model, the repassivation kinetics of materials was not affected by the multiple particle impingements, i.e. particle concentration in slurry. Actually, the active area produced by the breakdown of the passive film and the still passive area can be approximately treated as a galvanic couple. The polarization of the galvanic couple would be affected by

the increasing of the fraction of the active area. Due to this, the open circuit potential of passive targets will shift negatively with an increasing concentration of solid particles in flowing slurries [10].

5.4.3 Mechanical properties of target materials and solid particles

The effects of mechanical properties of materials and solid particles on erosion-corrosion have been discussed in **Section 2.4.1.3** and **Section 2.4.2.3**. To simplify our analysis and model, it is assumed that the size, shape and momentum of particles are identical and they are the same as the average values of sand particles. Moreover, it is assumed that the target surface is homogeneous, that the kinetic energy absorbed by the target material is equal to the energy required to create the crater by the particle impingement, resulting in an identical transient current response.

However, in reality, in the flowing slurry, the particles are likely to rebound after impacting the target material's surface. The kinetic energy of the particle and the absorbed energy by target material should be approximately equal to the difference between kinetic energy of particle right before and immediately after its impingement. A more complicated fluid dynamics analysis would be necessary to evaluate the impact rebounding of solid particles.

5.4.4 Effect of repeated impingements of solid particles

Mechanical and electrochemical properties can be influenced by the

repeated particle impingement on the same location of the target surface. This is due to a strain-hardening effect, especially at the initial stage of erosion. However, the failure of a slurry component often occurs after a long period of flowing. Before that, the strain hardening is saturated. The average current response during slurry erosion indicates that the current densities under the potentiostatic control are not initially stable due to the change of surface roughness and mechanical properties. After a given time, the system reaches a stable state of erosion-corrosion, i.e. the surface roughness reaches a saturated value and the formation rate of the hardened layer is equal to the thickness loss rate caused by the erosion-corrosion process. In the whole erosion-corrosion process of present study, the initial stage is rather short, and the system is mainly under the stable condition. To simplify the model, only the stable state is considered, and the effect of repeated impingement is theoretically negligible.

5.4.5 Corrosion-enhanced erosion

As indicated in **Section 2.3.2**, corrosion could influence erosion by lowering a surface's mechanical properties [10,13,19,22,23,24,25,26]. Lu *et al.* [13] even predicted a theoretical model to correlate the anodic current density to the corrosion-enhanced erosion rate, as follows:

$$\frac{e_c}{e_0} = Z \log\left(\frac{i_a}{i_{th}}\right) \qquad (2\text{-}9)$$

where e_0 is the pure erosion rate, and i_{th} is the threshold anodic current density to cause the corrosion-enhanced erosion. By correlating **Eq. 2-9** to the theoretical models of mechanical erosion, these models can be used to predict the erosion behaviour of metals in corrosive slurries. As a result, we can predict the erosion-enhanced corrosion more accurately by taking the effect of corrosion-enhanced erosion into account.

5.5 Conclusions

1. The corrosion of a passive metal in flowing slurry is mainly controlled by the rate of generation of an active area caused by particle impingement and repassivation kinetics of the active area.
2. The new model successfully predicts the corrosion rate of passive targets that display different kinetics behaviour of repassivation.
3. The use of kinetic parameters of repassivation determined from scratch tests slightly overestimates the current densities in flowing slurry.

References

[1] D. C. Silverman, "The rotating cylinder electrode for examining velocity-sensitive corrosion - A review", Corrosion, 60 (2004), pp. 1003-1024.

[2] J. Postlethwaite, M. H. Dobbin and K. Bergevin, "Role of Oxygen Mass Transfer in the Erosion-Corrosion of Slurry Pipe Lines", Corrosion, 42 (1986), pp.514-521.

[3] T. Y. Chen, A. Moccari, D. D. Macdonna, MTI Publication, No. T-3, Materials technology Institute of the Chemical Process Industries, Inc., 1992.

[4] B. Poulson, "Electrochemical Measurements in Flowing Solutions", Corrosion Science 23 (4) (1983), pp. 391-430.

[5] E. Heitz, "Chemo-mechanical effects of flow on corrosion", Corrosion 47 (2) (1991), pp.135-145.

[6] G.T. Burstein, K. Sasaki, "Detecting electrochemical transients generated by erosion-corrosion", Electrochimica Acta 46 (2001), pp. 3675-3683.

[7] X. Hu and A. Neville, "The electrochemical response of stainless steels in liquid-solid impingement", Wear 258 (2005), pp.641-648.

[8] I. Garcia, D. Drees, and J. P. Celis, "Corrosion-wear of passivating materials in sliding contacts based on a concept of active wear track area", Wear 249 (2001), pp. 452-460.

[9] R. J. K. Wood, J. A. Wharton, A. J. Speyer, and K. S. Tan, "Investigation of erosion-corrosion processes using electrochemical noise measurements", Tribology International 35 (2002), pp. 631-641.

[10] M. Matsumura, Y. Oka, H. Hiura, and M. Yano, "The role of passivating film in preventing slurry erosion-corrosion austenitic stainless steel", ISIJ Int. 31 (2) (1991), pp. 168-176.

[11] J. Li, Y.G. Zheng, J.Q. Wang, Z.M. Yao, Z. Wang, F, W. Ke, "Depassivation and repassivation of AISI321 stainless steel surface during solid particle impact in 10% H2SO4 solution", Wear 186-187 (1995), pp.562-567.

[12] X.Z. Zhao, N. Cui, J.L. Luo, S. Chiovelli, "Effects of erosion on

corrosion of type 430 and 316 stainless steels in aqueous environments", British Corrosion Journal 37 (1) (2002), pp. 63-68.

[13] B.T. Lu, J.L. Luo, "Synergism of electrochemical and mechanical factors in erosion - corrosion", Journal of Physical Chemistry B, (2006), pp. 4217-4231.

[14] B. T. Lu And J. L. Luo: Effects of Slurry Chemistry on Corrosion-Enhanced Erosion of Carbon Steel, to be presented at Corrosion 2008.

[15] F. Ferrer, H. Idrissi, H. Mazzile, P. Fleischmann, P. Labbeeuw, "On the potential of acoustic emission for the characterization and understanding of mechanical damaging during abrasion-corrosion processes", Wear 231 (1999), pp. 108-115.

[16] A. Neville and X. Hu, "Assessment of electrochemical response from high alloy stainless steels during slurry impingement and single impacts to improve understanding of erosion-corrosion", British Corrosion Journal 37 (2002), pp. 43-47.

[17] B.T. Lu, J.L. Luo, F. Mohammadi, K.Wang, X.M.Wan, "Correlation between repassivation kinetics and corrosion rate over a passive surface in flowing slurry", Electrochimica Acta 53 (2008), pp. 7022-7031.

[18] B.T. Lu, J.L. Luo, H.Y. Ma, "A theoretical model on electrochemical response of passivated metals to solid particle impingement", Journal of The Electrochemical Society 154 (3) (2007), pp. 159-168.

[19] J. Postlethwaite, "Components of erosion-corrosion in aqueous slurries of sand " Corrosion 37 (1) (1981), pp. 1-5.

[20] H.X. Guo, B.T. Lu, J.L. Luo, "Study on passivation and erosion-enhanced

corrosion resistance by Mott-Schottky analysis", Electrochimica Acta 52 (2006), pp. 1108–1116.

[21] A.W. Hassel, A.J. Smith, "Single particle impact experiments for studying particle induced flow corrosion", Corrosion Science 49 (2007), pp. 231-239.

[22] W. Tsai, J.A.C. Humphrey, I. Cornet, A. Levy, "Experimental measurement of accelerated erosion in a slurry pot tester", Wear 68 (1981), pp. 289-303.

[23] Y. Li, G.T. Burstein, I.M. Hutchings, "The influence of corrosion on the erosion of aluminium by aqueous silica slurries", Wear 186 (2) (1995), p. 515.

[24] J.A. Bester, A. Ball, "Performance of aluminum alloys and particulate reinforced aluminum metal matrix composites in erosive-corrosive slurry environments", Wear 162–164 (1993), pp. 57-63.

[25] M. Reyes, A. Neville, "Mechanisms of erosion-corrosion on a cobalt-base alloy and stainless-steel UNS S17400 in aggressive slurries", Journal of Materials Engineering and Performance 10 (6) (2001), pp. 723-730.

[26] H.X. Guo, B.T. Lu, J.L. Luo, "Response of surface mechanical properties to electrochemical dissolution determined by in situ nanoindentation technique", Electrochemistry Communications, v8, pp. 1092-1098.

Chapter 6

Summary and Future Work

6.1 Contribution to knowledge

In the present work, erosion-corrosion behaviour and surface degradation were investigated, and a modified model was developed to predict the average current density in the erosion-corrosion process. The main contributions to knowledge are summarized as follows:

1. **Influence of chemical composition on the erosion-corrosion process**

The present study listed the influences of the chemical composition of neutral, alkaline and acid solutions on erosion-corrosion. In order to fully understand this effect and to compare erosion-corrosion on the same level, all experiments were controlled under the same galvanostatic condition, i.e. the same applied current density. Between acid solutions, the erosion-corrosion process and surface mechanical degradation varied remarkably; hence more attempts have been made to investigate the phenomenon in acid solutions. However, the mechanism of severe erosion-corrosion and surface degradation in acid solutions is not clearly understood.

2. Correlation of erosion-corrosion and surface degradation

Nanoindentation tests were preformed to investigate surface degradation in neutral, alkaline and acid solutions. They indicate that with the existence of corrosion, higher erosion rates correspond to a more severe surface degradation. Therefore, it could be concluded that surface degradation might be at least one of the mechanisms causing an additional erosion rate.

3. Development of an erosion-corrosion model

In a static passive system, the material surface is covered by a protective passive surface film which prevents corrosion. When in a flowing slurry, the passive film can be broken down by the impingements of flowing particles, which causes an additional corrosion current. This model was developed to predict this average corrosion current in a passive system with flowing slurry by repassivation kinetics. This model can give reasonable predictions on the corrosion current, while it overestimates the corrosion current. More accurate corrections should be made on this model.

6.2 Contribution to literature

Based on the experimental results and analysis conducted in this work, the following papers have been published, accepted for publication, or are in preparation.

(1) K. Wang, B.T. Lu and J.L. Luo, "Surface hardness-degradation of iron in corrosion media with different pHs," 2008 NACE Northern Area Western Conference, Edmonton, February 11-14, 2008.

(2) B.T. Lu, K. Wang, X.M. Wan and J.L. Luo, "Effects of slurry pH on the surface mechanical properties and erosion-corrosion resistance," Corrosion/2008, Paper No. 08668, NACE, Houston.

(3) B.T. Lu, J.L. Luo, F. Mohammadi, K. Wang and X.M. Wan, "Correlation between repassivation kinetic and corrosion rate over a passive surface in flowing slurry," ***Electrochimica Acta***, 53 (2008), pp. 7022-7031.

(4) K. Wang, B.T. Lu, and J.L. Luo, "Effect of solution composition on erosion corrosion and surface mechanical properties of Fe based alloy and iron," in preparation.

6.3 Contribution to Engineering

Based on the phenomena and predictions in Chapter 4 and Chapter 5, the present study could be used to evaluate erosion-corrosion problems occurring in industry.

1. **In Chapter 4**, it was discussed that erosion-corrosion depends on 1) whether the solution is acid and 2) the types of anions in a solution with presence of H^+. In this case, companies can roughly compare the erosion-corrosion rates of the same material in slurries with different solution compositions.
2. Also, **in Chapter 4**, it is confirmed that the erosion rate is inversely

proportional to surface hardness, i.e. for the same material, a higher erosion rate is due to a lower surface hardness. With this relationship, it is possible to compare the erosion rates of the same material by testing its *in-situ* surface hardness.

3. **Chapter 5** predicted the erosion model in a passive system to correlate the nominal current density to the repassivation kinetics. This prediction can be used to compare the erosion rates of the same material in a passive system by testing the erosion-corrosion current density. Or, knowing the erosion rate and response of current density, it can be used to predict another erosion rate by comparing the current density under another condition for the same material.

6.4 Suggestions for future work

Though many efforts have been made on investigating the erosion-corrosion behaviors and model prediction, some experimental phenomena and mechanisms are still not clear. Further investigations are required to clarify these phenomena. The suggestions are as follows:

1. **Mechanism of the chemical composition's effect on the erosion-corrosion process**

The present study has found that, even under the same galvanostatic control, the erosion-corrosion rate is higher in acidic solutions. Surface

degradation has been considered as one of the mechanisms, but not the only one. The hydrogen ion might be the reason, but this is not experimental evidence regarding that idea. More efforts should be made to investigate the other mechanisms why acid solutions result in more severe erosion-corrosion rate and surface degradation.

2. Improving the accuracy of the erosion-corrosion model

As mentioned in **Chapter 5**, even though the current model gives reasonable predictions regarding the corrosion current in passive system, it only considers the effect of erosion on corrosion. As a consequence, we could predict the erosion-enhanced corrosion in a more accurate way by taking the effect of corrosion-enhanced erosion into account.